

1      The effects of multi-dimensional drought on land cover change and  
2      vegetation productivity in continental Chile

3      Francisco Zambrano<sup>a,1,\*</sup>, Anton Vrieling<sup>b</sup>, Francisco Meza, Iongel Duran-Llacer, Francisco Fernández<sup>c</sup>,  
4      Alejandro Venegas-González, Nicolas Raab, Dylan Craven

<sup>a</sup> Universidad Mayor, Hémera Centro de Observación de la Tierra, Facultad de Ciencias, Escuela de Ingeniería en Medio Ambiente y Sustentabilidad, Santiago, Chile, 7500994

<sup>b</sup> University of Twente, Faculty of Geo-Information Science and Earth Observation (ITC), Enschede, The Netherlands,

<sup>c</sup> Universidad San Sebastián,

---

5      **Abstract**

The north-central region of Chile has been the focus of research studies due to the persistent decrease in water supply, which is impacting the hydrological system and vegetation development. This persistent period of water scarcity has been defined as a megadrought. The aim of our study is to evaluate the land cover change over continental Chile and to examine how this is connected to drought indices of water supply, atmospheric evaporative demand (AED), soil moisture, and their effects on vegetation productivity. The drought indices were derived using monthly ERA5-Land reanalysis data spanning from 1981 to 2023. The Moderate-Resolution Imaging Spectroradiometer (MODIS) datasets were utilized to obtain information on annual land cover and monthly vegetation productivity. We analyzed short- (1, 3, 6 months) to long-term (12, 24, 36 months) time scales of drought. Our results showed that land cover change was highest in the south-central part of the country, reaching changes as high as 36% in the surface type. The water demand has increased for the whole country, with a major increase in the north. The AED and soil moisture evidence a decreasing trend, which decreases at longer time scales and from north to south. The extreme south part of the country shows an increase in supply. Vegetation productivity has a negative trend in the north-central region for all land cover types. On the other hand, forests seem to be the most resistant type to drought. The types that show to be most affected by variation in climate conditions are shrublands, savannas, and croplands. The drought indices that have the capability of explaining to a major degree the variance in vegetation productivity are the ones that consider soil moisture for twelve months and the combined effect of precipitation and AED for 24 and 12 months. The results indicate that the north-central region is the most sensitive to water supply deficits lasting longer than a year.

6      **Keywords:** drought, land cover change, vegetation productivity, satellite

---

7      **1. Introduction**

8      Drought is often classified as meteorological when there is a decrease in precipitation below the mean  
9      average of several years (more than 30 years), hydrological when these anomalies last for long periods (months  
10     to years) and affect water systems, and agricultural when the deficit impacts plant health anomalies and  
11     leads to decreased productivity (Wilhite and Glantz, 1985). However, it is important to note that drought

---

\*Corresponding author

Email addresses: francisco.zambrano@umayor.cl (Francisco Zambrano), a.vrieling@utwente.nl (Anton Vrieling), francisco.fernandez@uss.cl (Francisco Fernández)

<sup>1</sup>This is the first author footnote.

is also influenced by human activities, which were not considered in the definitions. Thus, Van Loon et al. (2016) and AghaKouchak et al. (2021) have given an updated definition of drought for the Anthropocene, suggesting that it should be considered the feedback of humans' decisions and activities that drives the anthropogenic drought. Simultaneously, drought leads to heightened tree mortality and induces alterations in land cover and land use, ultimately affecting ecosystems (Crausbay et al., 2017). Even though many ecological studies have misinterpreted how to characterize drought, for example, sometimes considering "dry" conditions as "drought" (Slette et al., 2019). Then, Crausbay et al. (2017) proposed the ecological drought definition as "an episodic deficit in water availability that drives ecosystems beyond thresholds of vulnerability, impacts ecosystem services, and triggers feedback in natural and/or human systems." In light of current global warming, it is crucial to study the interaction between drought and ecosystems in order to understand their feedback and impact on water security. (Bakker, 2012)

Human-induced greenhouse gas emissions have increased the frequency and/or intensity of drought as a result of global warming, according to the sixth assessment report (AR6) of the Intergovernmental Panel on Climate Change (IPCC) (Calvin et al., 2023). The evidence supporting this claim has been strengthened since AR5 (IPCC, 2013). Recent studies, however, have produced contrasting findings, suggesting that drought has not exhibited a significant trend over the past forty years. (Vicente-Serrano et al., 2022; Kogan et al., 2020). Vicente-Serrano et al. (2022) analyzed the meteorological drought trend on a global scale, finding that only in a few regions has there been an increase in the severity of drought. Moreover, they attribute the increase in droughts over the past forty years solely to an increase in atmospheric evaporative demand (AED), which in turn enhances vegetation water demand, with important implications for agricultural and ecological droughts. Also, they state that "the increase in hydrological droughts has been primarily observed in regions with high water demand and land cover change". Similarly, Kogan et al. (2020) analyzed the drought trend using vegetation health methods, finding that for the globe, hemispheres, and main grain-producing countries, drought has not expanded or intensified for the last 38 years. Further, Masson-Delmotte (2021) suggests that there is a high degree of confidence that rising temperatures will increase the extent, frequency, and severity of droughts. Also, AR6 (Calvin et al., 2023) predicts that many regions of the world will experience more severe agricultural and ecological droughts even if global warming stabilizes at 1.5°–2°C. To better evaluate the impact of drought trends on ecosystems, assessments are needed that relate meteorological and soil moisture variables to their effects on vegetation.

From 1960 to 2019, land use change has impacted around one-third of the Earth's surface, which is four times more than previously thought (Winkler et al., 2021). Multiple studies aim to analyze and forecast changes in land cover globally (Winkler et al., 2021; Song et al., 2018) and regionally (Chamling and Bera, 2020; Homer et al., 2020; Yang and Huang, 2021). Some others seek to analyze the impact of land cover change on climate conditions such as temperature and precipitation (Luyssaert et al., 2014; Pitman et al., 2012). There is less research on the interaction between drought and land cover change (Chen et al., 2022; Akinyemi, 2021; Peng et al., 2017). Peng et al. (2017) conducted a worldwide investigation utilizing net primary production to examine the spatial and temporal variations in vegetation productivity at global level. The study aimed to assess the influence of drought by comparing the twelve-month Standardized Precipitation Evapotranspiration Index (SPEI) and land cover change. According to their findings, drought is responsible for 37% of the decline in vegetation productivity, while water availability accounts for 55% of the variation. Chen et al. (2022) studied the trend of vegetation greenness and productivity and its relation to meteorological drought (SPEI of twelve months in December) and soil moisture at the global level. The results showed lower correlations (<0.2) for both variables. Akinyemi (2021) evaluates drought trends and land cover change using vegetation indices in Botswana in a semi-arid climate. These studies mostly looked at how changes in land cover and vegetation productivity are related to a single drought index (SPEI) over a single time period of 12 months. SPEI takes into account the combined effect of precipitation and AED as a water balance, but it does not allow us to know the contribution of each variable on its own. Some things worth investigating in terms of land cover change and vegetation productivity are: i) How do they respond to short- to long-term meteorological and soil moisture droughts? ii) How is the drought impacting land cover changes? And iii) How do they behave in humid and arid climatic zones regarding drought? Likewise, there is a lack of understanding of how the alteration in water supply and demand is affecting land cover

63 transformations.

64 For monitoring drought, the World Meteorological Organization recommends the SPI (Standardized Pre-  
65 cipitation Index) (WMO et al., 2012). The SPI is a multi-scalar drought index that only uses precipitation  
66 to assess short- to long-term droughts. The primary cause of drought is precipitation anomalies, and tem-  
67 perature usually makes it worse (Luo et al., 2017). Nowadays, there is an increase in attention toward  
68 using AED separately to monitor droughts (Vicente-Serrano et al., 2020). One reason is due to its attri-  
69 bution to increasing flash droughts in water-limited regions (Noguera et al., 2022). Vicente-Serrano et al.  
70 (2010) proposed the Standardized Precipitation Evapotranspiration Index (SPEI), which incorporated the  
71 temperature effect by subtracting AED from precipitation. SPEI allows for analysis of the combined effect  
72 of precipitation and AED. Since its formulation, it has been used worldwide for the study and monitoring  
73 of drought (Gebrechorkos et al., 2023; Liu et al., 2024). Hobbins et al. (2016) and McEvoy et al. (2016)  
74 developed the Evaporative Demand Drought Index (EDDI) to monitor droughts solely using the AED, and  
75 it has proven effective in monitoring flash droughts (Li et al., 2024; Ford et al., 2023). For soil moisture,  
76 several drought indices exist, such as the Soil Moisture Deficit Index (SDMI) (Narasimhan and Srinivasan,  
77 2005) and the Soil Moisture Agricultural Drought Index (SMADI) (Souza et al., 2021). Hao and AghaK-  
78 ouchak (2013) and AghaKouchak (2014) proposed the Standardized Soil Moisture Index (SSI), which has a  
79 similar formulation as the SPI, SPEI, and EDDI. Thus, there are plenty of drought indices that allow for  
80 a comprehensive assessment of drought on short- to long-term scales and that allow for the use of single  
81 variables from the earth's water balance (e.g., precipitation, AED, soil moisture). The variation in climate  
82 variables impacts vegetation development, and unfavorable conditions such as low precipitation and high  
83 temperatures usually generate a decrease in vegetation productivity. To monitor the response of vegetation,  
84 the common practice is to use satellite data. The Normalized Difference Vegetation Index (NDVI) has been  
85 widely used as a proxy for biomass production (Camps-Valls et al., 2021; Paruelo et al., 2016; Helman et al.,  
86 2014). For Chile's cultivated land, Zambrano et al. (2018) introduced the zcNDVI for assessing seasonal  
87 biomass production in response to drought. Using this information, we can advance our understanding of  
88 the impact of drought on ecosystems.

89 Chile's diverse climatic and ecosystem types (Beck et al., 2023; Luebert and Pliscoff, 2022) make it an ideal  
90 natural laboratory for studying climate and ecosystems. Additionally, the country has experienced severe  
91 drought conditions that have had significant effects on vegetation and water storage. North-central Chile has  
92 faced a persistent precipitation deficit since 2010, defined as a mega drought. (Garreaud et al., 2017), which  
93 has impacted the Chilean ecosystem. This megadrought was defined by the Standardized Precipitation  
94 Index (SPI) of twelve months in December having values below one standard deviation. Some studies have  
95 addressed how this drought affects single ecosystems in terms of forest development (Miranda et al., 2020;  
96 Venegas-González et al., 2018), forest fire occurrence (Urrutia-Jalabert et al., 2018), and crop productivity  
97 (Zambrano, 2023; Zambrano et al., 2018, 2016). We found one study regarding land cover and drought in  
98 Chile. The study by Fuentes et al. (2021) evaluates water scarcity and land cover change in Chile between  
99 29° and 39° of south latitude. Fuentes et al. (2021) used the SPEI of one month for evaluating drought,  
100 which led to misleading results. For example, they did not find a temporal trend in the SPEI but found a  
101 decreasing trend in water availability and an increase trend on AED, which in turn should have been capable  
102 of being captured with longer time scales of the SPEI. The term "megadrought" in Chile is used to describe  
103 a prolonged water shortage that lasts for several years, resulting in a permanent deficit that impacts the  
104 hydrological system (Boisier et al., 2018). Therefore, it is crucial to evaluate temporal scales that consider  
105 the cumulative impact over a period of several years. The association between drought and the environment  
106 in Chile is not well comprehended. Hence, it is imperative to acquire a more profound comprehension of the  
107 manner in which climatic and soil moisture droughts influence environmental dynamics, in order to make  
108 well-informed decisions on adaptation strategies.

109 Here, we analyze the multi-dimensional impacts of drought across ecosystems in continental Chile. More  
110 specifically, we aim to assess: i) short- to long-term temporal trends in multi-scalar drought indices; ii)  
111 temporal changes in land-use cover and the direction and magnitude of their relationships with trends in  
112 drought indices; and iii) the trend in vegetation productivity and its relationship with drought indices across

<sup>113</sup> Chilean ecosystems.

## <sup>114</sup> 2. Study area

<sup>115</sup> Continental Chile has diverse climate conditions with strong gradients from north to south and east to west  
<sup>116</sup> (Aceituno et al., 2021) (Figure 1 a), which determines its great ecosystem diversity (Luebert and Pliscoff,  
<sup>117</sup> 2022) (Figure 1 c). The Andes Mountains are a main factor in climate latitudinal variation (Garreaud, 2009).  
<sup>118</sup> “Norte Grande” and “Norte Chico” predominate in an arid desert climate with hot (Bwh) and cold (Bwk)  
<sup>119</sup> temperatures. At the south of “Norte Chico,” the climate changes to an arid steppe with cold temperatures  
<sup>120</sup> (Bsk). In these two northern regions, the land is mostly bare, with a small surface of vegetation types  
<sup>121</sup> such as shrubland and grassland. In the zones “Centro” and the north half of “Sur,” the main climate is  
<sup>122</sup> Mediterranean, with warm to hot summers (Csa and Csb). Land cover in “Centro” comprises a significant  
<sup>123</sup> amount of shrubland and savanna (50%), grassland (16%), forest (8%), and croplands (5%). An oceanic  
<sup>124</sup> climate (Cfb) predominates in the south of “Sur” and the north of “Austral.” Those zones are high in forest  
<sup>125</sup> and grassland. The southern part of the country has a tundra climate, and in “Austral,” it is a cold semi-arid  
<sup>126</sup> area with an extended surface of grassland, forest, and, to a lesser extent, savanna.

## <sup>127</sup> 3. Materials and Methods

### <sup>128</sup> 3.1. Data

#### <sup>129</sup> 3.1.1. Gridded meteorological and vegetation data

<sup>130</sup> To analyze land cover change, we use the classification scheme by the IGBP (International Geosphere-  
<sup>131</sup> Biosphere Programme) from the product MCD12Q1 collection 6.1 from MODIS. The MCD12Q1 has a yearly  
<sup>132</sup> frequency from 2001 to 2022 and defines 17 classes. To derive a proxy for vegetation productivity, we used  
<sup>133</sup> the Normalized Difference Vegetation Index (NDVI) from the product MOD13A3 collection 6.1 from MODIS  
<sup>134</sup> (Didan, 2015). MOD13A3 provides vegetation indices at 1km of spatial resolution and monthly frequency.  
<sup>135</sup> The NASA EOSDIS Land Processes Distributed Active Archive Center (LP DAAC), USGS Earth Resources  
<sup>136</sup> Observation and Science (EROS) Center, Sioux Falls, South Dakota, provided the MOD13A3 and MCD12Q1  
<sup>137</sup> from the online Data Pool, accessible at <https://lpdaac.usgs.gov/tools/data-pool/>.

Table 1: Description of the satellite and reanalysis data used

Product	Sub-product	Variable	Spatial Resolution	Period	Units	Short Name
ERA5L		Precipitation	0.1°	1981-2023	mm	P
		Maximum temperature			°C	$T_{max}$
		Minimum temperature			°C	$T_{min}$
		Volumetric Soil Water Content at 1m			m3/m3	SM
ERA5L*	MOD13A3.061	Atmospheric Evaporative Demand	0.1°	1981-2023	mm	AED
MODIS		Normalized Difference Vegetation Index	1 km	2000-2023		NDVI
	MCD12Q1.061	land cover IGBP scheme		2001-2022		land cover

\*Calculated from maximum and minimum temperatures derived from ERA5L with Eq. 1.

<sup>138</sup> For soil moisture, water supply, and water demand variables, we used ERA5L (ECMWF Reanalysis version  
<sup>139</sup> 5 over land) (Muñoz-Sabater et al., 2021), a reanalysis dataset that provides the evolution of atmospheric and  
<sup>140</sup> land variables since 1950. It has a spatial resolution of 0.1° (9 km), hourly frequency, and global coverage.  
<sup>141</sup> We selected the variables for total precipitation, maximum and minimum temperature at 2 meters, and  
<sup>142</sup> volumetric soil water layers between 0 and 100cm of depth (layer 1 to layer 3). Table 1 shows a summary  
<sup>143</sup> of the data and its main characteristics.

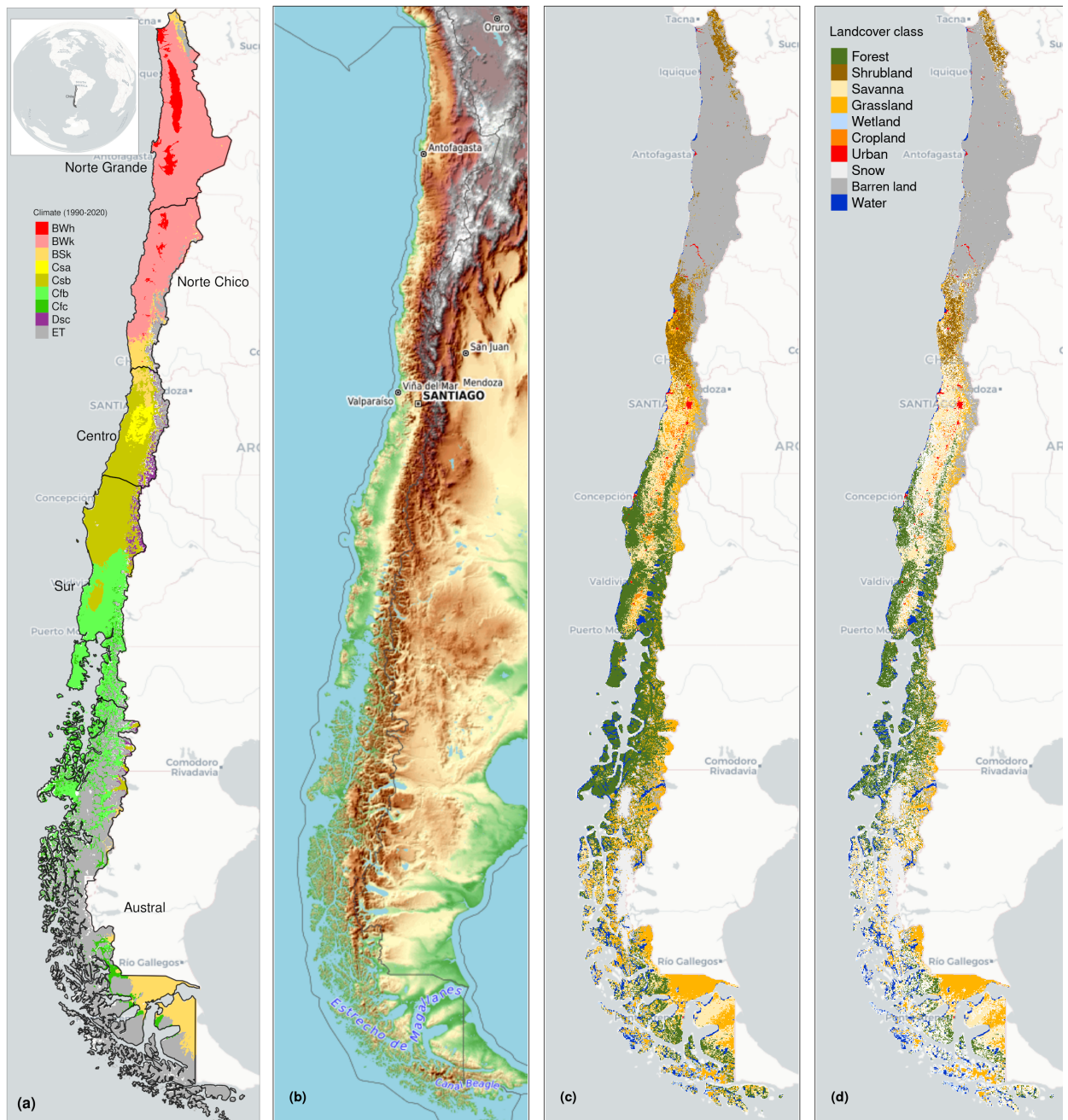


Figure 1: (a) Chile with the Koppen-Geiger climate classes and the five macrozones “Norte Grande”, “Norte Chico”, “Centro”, “Sur”, and “Austral”. (b) Topography reference map. (c) land cover classes for 2022. (d) Persistent land cover classes (> 80%) for 2001-2022

144 3.2. Short- to long-term drought trends

145 3.2.1. Atmospheric Evaporative Demand (AED)

146 In order to compute the drought indices that use water demand, it is necessary to first calculate the  
 147 AED. To do this, we employed the Hargreaves method ([Hargreaves, 1994](#); [Hargreaves and Samani, 1985](#)) by  
 148 applying the following equation:

$$AED = 0.0023 \cdot Ra \cdot (T + 17.8) \cdot (T_{max} - T_{min})^{0.5} \quad (1)$$

where  $Ra$  ( $MJ\ m^2\ day^{-1}$ ) is extraterrestrial radiation;  $T$ ,  $T_{max}$ , and  $T_{min}$  are mean, maximum, and minimum temperature ( $^{\circ}C$ ) at 2m. For calculating  $Ra$  we used the coordinate of the latitud of the centroid of each pixel. We chose the method of Hargreaves to estimate AED because of its simplicity, which only requires temperatures and extrarrestrial radiation. Also, it has been recommended over other methods (e.g., Penman-Monteith) when the access to climatic variables is limited (Vicente-Serrano et al., 2014).

### 3.2.2. Non-parametric calculation of drought indices

To derive the drought indices of water supply and demand, soil moisture, and vegetation (i.e., the proxy of productivity), we used the ERA5L dataset and the MODIS product, with a monthly frequency for 1981–2023 and 2000–2023, respectively. The drought indices correspond to a historical anomaly with regard to a variable (e.g., meteorological, vegetation, or soil moisture). To account for the anomaly, the common practice is to derive it following a statistical parametric methodology in which it is assumed that the statistical distribution of the data is known (Heim, 2002). A wrong decision is usually the highest source of uncertainty (Laimighofer and Laaha, 2022). In the case of Chile, due to its high degree of climatic variability, it is complex to choose a proper distribution without previous research. Here, we follow a non-parametric methodology for the calculation of the drought indices, in a similar manner as the framework proposed by Farahmand and AghaKouchak (2015); Hobbins et al. (2016); McEvoy et al. (2016).

For the purpose of monitoring water supply drought, we used the well-known Standardized Precipitation Index (SPI), which relies on precipitation data. To evaluate water demand, we chose the Evaporative Demand Drought Index (EDDI), developed by Hobbins et al. (2016) and McEvoy et al. (2016), which is based on the AED. The United States currently monitors drought using the EDDI (<https://psl.noaa.gov/eddi/>) as an experimental index. To consider the combined effect of water supply and demand, we selected the SPEI (Vicente-Serrano et al., 2010). For SPEI, an auxiliary variable  $D = P - AED$  is calculated. Soil moisture is the main driver of vegetation productivity, particularly in semi-arid regions (Li et al., 2022). Hence, for soil water drought, we used the SSI (Standardized Soil Moisture Index) (Hao and AghaKouchak, 2013; AghaKouchak, 2014). In our case, for the SSI, we used the average soil moisture from ERA5L at 1m depth. Finally, for the proxy of productivity, we used the zcNDVI proposed by Zambrano et al. (2018), which was derived from the monthly time series of NDVI retrieved from MOD13A1. All the indices are multi-scalar and can be used for the analysis of short- to long-term droughts.

To derive the drought indices, first we must calculate the sum of the variables with regard to the time scale (s). In this case, for generalization purposes, we will use  $V$ , referring to variables  $P$ ,  $AED$ ,  $D$ ,  $NDVI$ , and  $SM$  (Table 1). We cumulated each  $V$  over the time series of  $n$  values (months), and for the time scales  $s$ :

$$A_{si} = \sum_{i=n-s-i+2}^{n-i+1} V_i \quad \forall i \geq n - s + 1 \quad (2)$$

The  $A_{si}$  corresponds to a moving window (convolution) that sums the variable for time scales  $s$  from the last month, month by month, until the first month in which it could sum for  $s$  months. An inverse normal approximation (Abramowitz and Stegun, 1968) obtains the empirically derived probabilities once the variable cumulates over time for the scale  $s$ . Then, we used the empirical Tukey plotting position (Wilks, 2011) over  $A_i$  to derive the  $P(a_i)$  probabilities across a period of interest:

$$P(A_i) = \frac{i - 0.33}{n + 0.33'} \quad (3)$$

The drought indices  $SPI$ ,  $SPEI$ ,  $EDDI$ ,  $SSI$ , and  $zcNDVI$  are obtained following the inverse normal approximation:

$$DI(A_i) = W - \frac{C_0 + C_1 \cdot W + c_2 \cdot W^2}{1 + d_1 \cdot W + d_2 \cdot W^2 + d_3 \cdot W^3} \quad (4)$$

187  $DI$  is referring to the drought index calculated for the variable  $V$  (i.e., SPI, SPEI, EDDI, SSI, and zcNDVI).  
 188 The values for the constats are:  $C_0 = 2.515517$ ,  $C_1 = 0.802853$ ,  $C_2 = 0.010328$ ,  $d_1 = 1.432788$ ,  $d_2 =$   
 189  $0.189269$ , and  $d3 = 0.001308$ . For  $P(A) \leq 0.5$ ,  $W = \sqrt{-2 \cdot \ln(P(A_i))}$ , and for  $P(A_i) > 0.5$ , replace  $P(A_i)$   
 190 with  $1 - P(A_i)$  and reverse the sign of  $DI(A_i)$ .

191 The drought indices were calculated for time scales of 1, 3, 6, 12, 24, and 36 months at a monthly frequency  
 192 for 1981–2023 in order to be used for short- to long-term evaluation of drought. In the case of the proxy of  
 193 vegetation productivity (zcNDVI), it was calculated for a time scale of six months at monthly frequency for  
 194 2000–2023. For zcNDVI, we test time scales of 1, 3, 6, and 12 months in December and its correlation with  
 195 net primary production (NPP) obtained from the MOD17A3HGF product from MODIS. We choose to use  
 196 six months because r-squared with NPP increases from one to six months and from six to 12 months has  
 197 little improvement (see supplementary material in Section S5).

### 198 3.2.3. Trend of drought indices

199 To estimate if there are significant positive or negative trends for the drought indices, we used the non-  
 200 parametric test of Mann-Kendall ([Kendall, 1975](#)). To determine the magnitude of the trend, we used Sen's  
 201 slope ([Sen, 1968](#)). Some of the advantages of applying this methodology are that the Sen's slope is not  
 202 affected by outliers as regular regression does, and it is a non-parametric method that is not influenced by  
 203 the distribution of the data. We applied Mann-Kendall to see if the trend was significant and Sen's slope  
 204 to estimate the magnitude of the trend. We did this to the six time scales from 1981 to 2023 (monthly  
 205 frequency) and the indices SPI, EDDI, SPEI, and SSI. Thus, we have trends per index and time scale (24 in  
 206 total). Then, we extracted the trend aggregated by macrozone and per land cover persistent macroclasses.

### 207 3.3. Interaction of land cover and drought

#### 208 3.3.1. Land cover change

209 To analyze the land cover change, we use the IGBP scheme from the MCD12Q1 collection 6.1 from MODIS.  
 210 This product has been previously used for studies of drought and land cover in Chile ([Fuentes et al., 2021](#);  
 211 [Zambrano et al., 2018](#)). From the 17 classes, we regrouped into ten macroclasses, as follows: classes 1-4 to  
 212 forest, 5-7 to shrublands, 8-9 to savannas, 10 as grasslands, 11 as wetlands, 12 and 14 to croplands, 13 as  
 213 urban, 15 as snow and ice, 16 as barren, and 17 to water bodies. Thus, we have a land cover raster time series  
 214 with the ten macroclasses for 2001 and 2023. We validate the land cover macroclasses regarding a highly  
 215 detailed (30 m of spatial resolution) land cover map made for Chile by [Zhao et al. \(2016\)](#) for 2013-2014.  
 216 Our results showed a global accuracy of ~0.82 and a F1 score of ~0.66. Section S2 in the Supplementary  
 217 Material shows the procedure for validation.

218 We calculated the surface occupied per land cover class into the five macrozones (“Norte Grande” to  
 219 “Austral”) per year for 2001–2023. After that, we calculated the trend’s change in surface per land cover  
 220 type and macroclass. We used Mann-Kendall for the significance of the trend ([Kendall, 1975](#)) and Sen's  
 221 slope to calculate the magnitude ([Sen, 1968](#)).

222 Later in this study, we will examine the variation in vegetation productivity across various land cover  
 223 types and how water demand and supply, and soil moisture affect it. In order to avoid variations due to a  
 224 change in the land cover type from year-to-year that will wrongly impact NDVI, we developed a persistence  
 225 mask for land cover for 2001–2022. Thereby, we reduce an important source of variation on a regional  
 226 scale. Therefore, we generated a raster mask for IGBP MODIS per pixel using macroclasses that remained  
 227 unchanged for at least 80% of the years (2001–2022). This enabled us to identify regions where the land  
 228 cover macroclasses are persistent.

229    3.3.2. *Relationship between land cover and drought trends*

230    We wanted to explore the relationship between the trend in land cover classes and the trend in the drought  
231 indices. For this purpose, in order to have more representative results, we conducted the analysis over sub-  
232 basins within continental Chile. We use 469 basins, which have a surface area between 0.0746 and 24,000  
233 ( $km^2$ ), and a median area of 1,249 ( $km^2$ ). For each basin, we calculate the relative trend per land cover  
234 type, considering the proportion of the type relative to the total surface of the basin. Then, we extracted  
235 per basin the average trend of the drought indices SPI, SPEI, EDDI, SSI, and all their time scales 1, 3, 6,  
236 12, 24, and 36. Also, we extracted the average trend in the proxy of vegetation productivity (zcNDVI). We  
237 wanted to analyze which drought indices and time scales have a major impact on changes in land cover type.

238    We have 25 predictors, including drought indices and vegetation productivity. We analyzed the 25 predictors  
239 per type of landcover, thus running six random forest models. Random forest uses multiple decision  
240 trees and allows for classification and regression. Some advantages are that it allows to find no linear re-  
241 lationship, reduces overfitting, and allows to derive the variable importance. We used random forests for  
242 regression and trained 1000 forests. To obtain more reliable results, we resampled by creating ten folds,  
243 running a random forest per fold, and calculating the r-squared (rsq), root mean square error (RMSE), and  
244 variable importance.

245    The variable importance helps for a better understanding of the relationships by finding which variable has  
246 a higher contribution to the model. We calculate the variable's importance by permuting out-of-bag (OOB)  
247 data per tree and computing the mean standard error in the OOB. After permuting each predictor variable,  
248 we repeat the process for the resting variable. We repeated this process ten times (per fold) to obtain the  
249 performance metrics (rsq, RMSE, and variable importance).

250    3.4. *Drought impacts on vegetation productivity*

251    We analyzed the trend of vegetation productivity over the unchanged land cover macroclasses. To achieve  
252 this, we used the persistent mask of land cover macroclasses. This way, we tried to reduce the noise in the  
253 vegetation due to a change in land cover from year to year. We used the zcNDVI as a proxy of vegetation  
254 productivity. In Chile's cultivated land, [Zambrano et al. \(2018\)](#) introduced the zcNDVI for assessing seasonal  
255 biomass production in relation to climate.

256    We examine the drought indices of water demand, water supply, and soil moisture and their correlation  
257 with vegetation productivity. The objective is to determine the impact of soil moisture and water demand  
258 and supply on vegetation productivity. We want to address three main questions: Which of the drought  
259 variables—supply, demand, or soil moisture—most helps to explain the changes in plant productivity? How  
260 do the short- to long-term time scales of the drought variable affect vegetation productivity in Chile? And  
261 finally, how strong is the relationship between the variables and the drought index? Thus, we will be able to  
262 advance in understanding how climate is affecting vegetation, considering the impact on the five land cover  
263 types: forest, cropland, grassland, savanna, and shrubland.

264    We conducted an analysis on the linear correlation between the indices SPI, SPEI, EDDI, and SSI over  
265 time periods of 1, 3, 6, 12, 24, and 36 months with zcNDVI. We used a method similar to that used by  
266 [Meroni et al. \(2017\)](#) which compared the SPI time-scales with the cumulative FAPAR (Fraction of Absorbed  
267 Photosynthetically Active Radiation). We performed a pixel-to-pixel linear correlation analysis for each  
268 index within the persistent mask of land cover macroclasses. We first compute the Pearson coefficient of  
269 correlation for each of the six time scales. A time scale is identified as the one that attains the highest  
270 correlation ( $p < 0.05$ ). We then extracted the Pearson correlation coefficient corresponding to the time  
271 scales where the value peaked. As a result, for each index, we generated two raster maps: 1) containing  
272 the raster with values of the time scales and drought index that reached the maximum correlation, and 2)  
273 having the magnitude of the correlation obtained by the drought index at the time scales.

274    3.5. *Software*

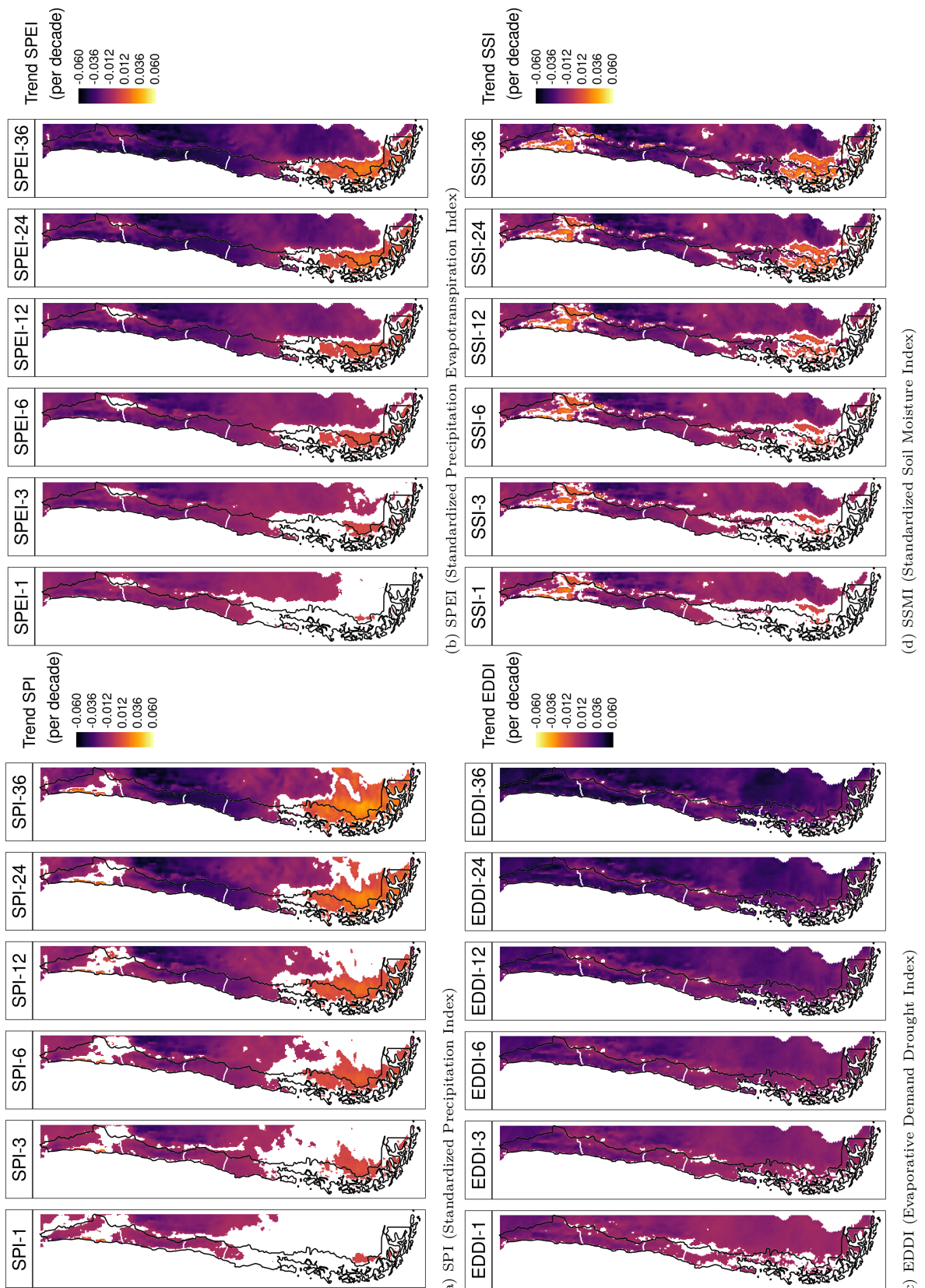
275    For the downloading, processing, and analysis of the spatio-temporal data, we used the open source software  
276 for statistical computing and graphics, R ([R Core Team, 2023](#)). For downloading ERA5L, we used the

277 `{ecmwfr}` package (Hufkens et al., 2019). For processing raster data, we used `{terra}` (Hijmans, 2023) and  
278 `{stars}` (Pebesma and Bivand, 2023). For managing vectorial data, we used `{sf}` (Pebesma, 2018). For  
279 the calculation of AED, we used `{SPEI}` (Beguería and Vicente-Serrano, 2023). For mapping, we use `{tmap}`  
280 (Tennekes, 2018). For data analysis and visualization, the suite `{tidyverse}` (Wickham et al., 2019) was used.  
281 For the random forest modeling, we used the `{tidymodels}`(Kuhn and Wickham, 2020) and `{ranger}`(Wright  
282 and Ziegler, 2017) packages.

283 **4. Results**

284 *4.1. Short- to long-term drought trends*

285 Figure 2 shows the spatial variation of the trend for the drought indices from short- to long-term scales.  
286 SPI and SPEI have a decreasing trend from “Norte Chico” to “Sur.” However, there is an increasing trend  
287 in “Austral.” The degree of the trend is stronger at higher time scales. The SSI indicates that in “Norte  
288 Grande,” there are surfaces that have increased in the southwest part and in the northeast have decreased,  
289 and is shown for all time scales. Similar to SPI and SPEI, SSI decreases at higher time scales. EDDI showed  
290 a positive trend for the whole of continental Chile, with a higher trend toward the north and a descending  
291 gradient toward the south. The degree of trend increases at higher time scales.



(c) EDDI (Evaporative Demand Drought Index)

(d) SSMI (Standardized Soil Moisture Index)

Figure 2: Linear trend of the drought index (\*) at time scales of 1, 3, 6, 12, 24, and 36 months for 1981-2023

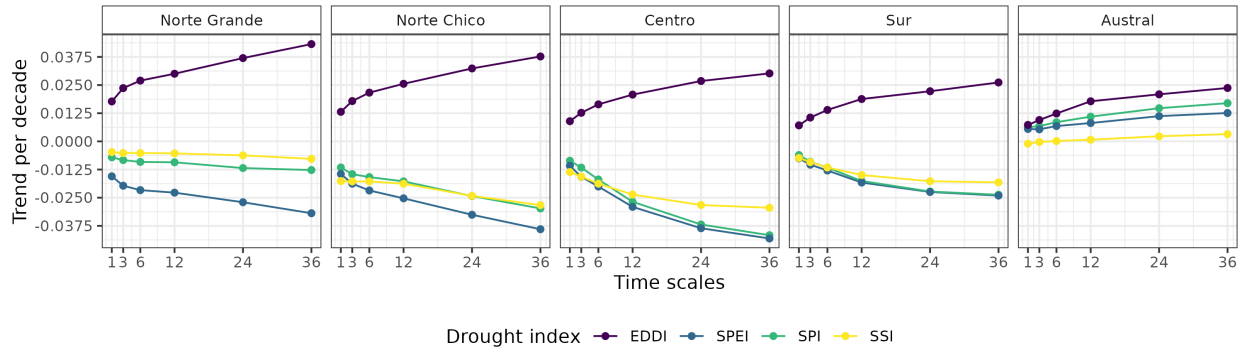


Figure 3: Trend per decade for the drought indices SPI, EDDI, SPEI, and SSI aggregated by macrozone.

The Figure 3 displays the averaged aggregation per macrozone, the drought index, and the timescale. The macrozones that reached the lowest trend for SPI, SPEI, and SSI are “Norte Chico” and “Centro,” where the indices also decrease at longer time scales. Potentially explained due to the prolonged reduction in precipitation that has affected the hydrological system in Chile. At 36 months, it reaches trends between -0.03 and -0.04 (z-score) per decade for SPI, SPEI, and SSI. For “Sur,” the behavior is similar, decreasing at longer scales and having between -0.016 and -0.025 per decade for SPI, SPEI, and SSI. “Norte Grande” has the highest trend at 36 months for EDDI (0.042 per decade), and “Centro” has the lowest for SPI and SPEI. In “Norte Grande” and “Norte Chico,” which are in a semi-arid climate, it is evident that the EDDI has an effect on the difference between the SPI and SPEI index, which is not seen in the other macrozones. Contrary to the other macrozones, “Austral” showed an increase in all indices, being the highest for EDDI at 36 months (0.025) and the lowest for SSI, which shows only a minor increase in the trend.

#### 4.2. Interaction of land cover and drought

##### 4.2.1. Land cover change

Table 2: Surface of the land cover class that persist during 2001-2022

Surface [km <sup>2</sup> ]						
macrozone	Forest	Cropland	Grassland	Savanna	Shrubland	Barren land
Norte Grande		886		7,910		171,720
Norte Chico		90	4,283	589	16,321	84,274
Centro	3,739	1,904	7,584	19,705	844	12,484
Sur	72,995	1,151	7,198	15,906		2,175
Austral	60,351		54,297	19,007	249	7,218
Total	—	137,085	3,145	74,247	55,206	25,324
						277,870

For vegetation, we obtained and use hereafter five macroclasses of land cover from IGBP MODIS: forest, shrubland, savanna, grassland, and croplands. Figure 1c shows the spatial distribution of the macroclasses through Chile for the year 2022. Figure 1d shows the macroclasses of land cover persistance (80%) during 2021–2022, respectively (Table 2). Within continental Chile, barren land is the land cover class with the highest surface area ( $277,870 \text{ km}^2$ ). The largest type of vegetation, with  $137,085 \text{ km}^2$ , is forest. Grassland has  $74,247 \text{ km}^2$ , savanna  $55,206 \text{ km}^2$ , shrubland  $25,324 \text{ km}^2$ , and cropland  $3,146 \text{ km}^2$  (Table 2). The macrozones with major changes for 2001–2022 were “Centro,” “Sur,” and “Austral,” with 36%, 31%, and 34% of their surface changing the type of land cover, respectively (Figure 1 and Table 3). Figure 4 shows the summary of the proportion of surface per land cover class and macrozone, derived from the persistance mask over continental Chile.

From the trend analysis in Table 3, we can indicate that the “Norte Chico” shows an increase in barren land of  $111 \text{ km}^2 \text{ yr}^{-1}$  and a reduction in the class savanna of  $70 \text{ km}^2 \text{ yr}^{-1}$ . In the “Centro” and “Sur,” there

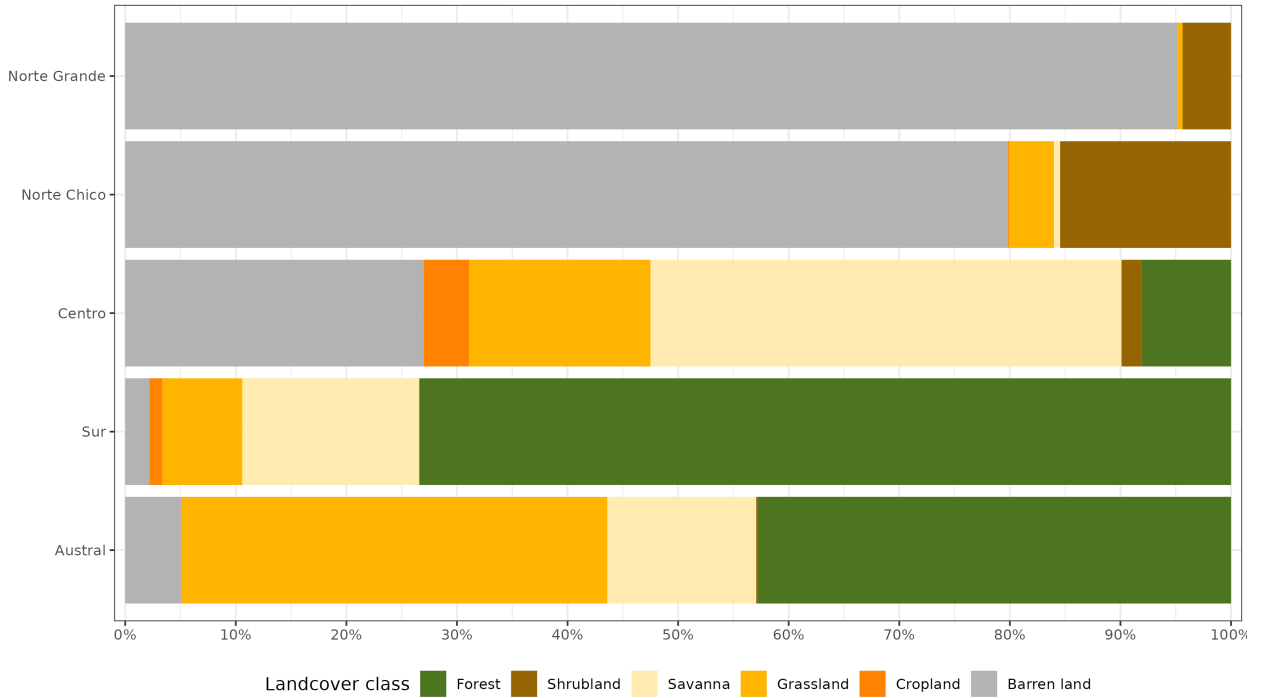
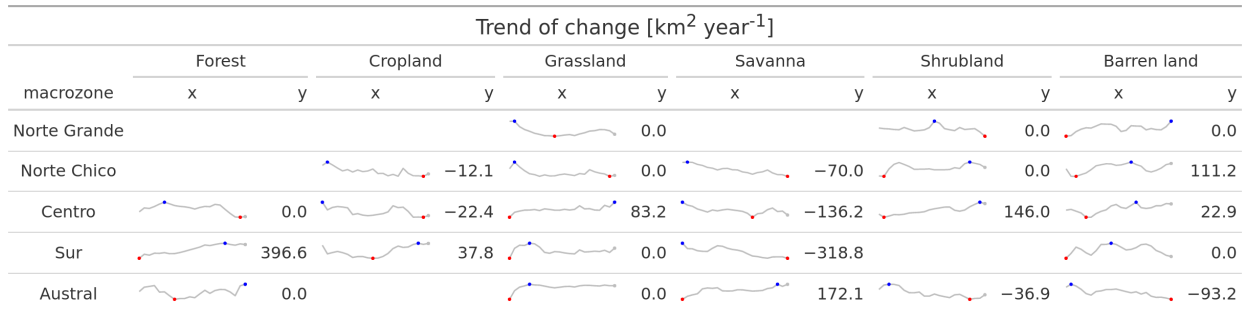


Figure 4: Proportion of land cover class from the persistent land cover for 2001-2022 (>80%) per macrozone

Table 3: The value of Sen's slope trend next to the time-series plot of surface per land cover class (IGBP MCD12Q1.016) for 2001–2022 through Central Chile. Values of zero indicate that there was not a significant trend. Red dots on the plots indicate the maximum and minimum values of surface.



are changes with an important reduction in savanna ( $136 \text{ to } 318 \text{ km}^2 \text{ yr}^{-1}$ ), and an increase in shrubland and grassland. Showing a change for more dense vegetation types. The area under cultivation (croplands) appears to be shifting from the “Centro” to the “Sur.” Also, there is a high increase in forest ( $397 \text{ km}^2 \text{ yr}^{-1}$ ) in the “Sur,” seemingly replacing the savanna lost (Table 3).

#### 4.2.2. Relationship between drought indices and land cover change

According to Table 4, the random forest models for estimating the landcover trend from the trends in drought indices reach an r-squared between 0.32 and 0.39 for the types of forest, grassland, savanna, shrubland, and barren land. It is more likely that short- and medium-term increases in AED (EDDI-6 and EDDI-12) and short-term precipitation deficits (SPI-6 and SPEI-6) contributed to changes in grassland and bare land. The short-term increase of AED (EDDI-3 and EDDI-6) and the longer duration of the precipitation deficit (SPI-24, SPI-36, and SPEI-36) most likely contribute to the changes in shrubland. The changes

Table 4: The five most important trends of drought indices in estimating the landcover trend per land cover type and the r-squared (rsq) reached by each random forest model.

Position	Forest (rsq=0.32)	Cropland (rsq=0.06)	Grassland (rsq=0.39)	Savanna (rsq=0.23)	Shrubland (rsq=0.23)	Barren_land (rsq=0.32)
1	EDDI-36	EDDI-36	EDDI-6	EDDI-6	EDDI-6	EDDI-12
2	EDDI-24	SSI-36	EDDI-12	EDDI-12	SPI-36	EDDI-6
3	EDDI-12	EDDI-24	EDDI-24	SPI-36	SPEI-36	SPI-6
4	SSI-36	EDDI-12	SPEI-6	EDDI-36	EDDI-3	SPEI-6
5	SSI-6	SSI-24	SPI-6	EDDI-24	SPI-24	EDDI-24

328 in savanna are associated with a short- and long-term increase in AED and a three-year precipitation deficit  
 329 (SPI-36). The increase in cumulative AED from 12 to 36 months is the strongest associated variable that  
 330 contributes to changes in forests, followed by the reduction of soil moisture over six and 36 months. The  
 331 supplementary material in Section S3 provides further details about the variable's importance.

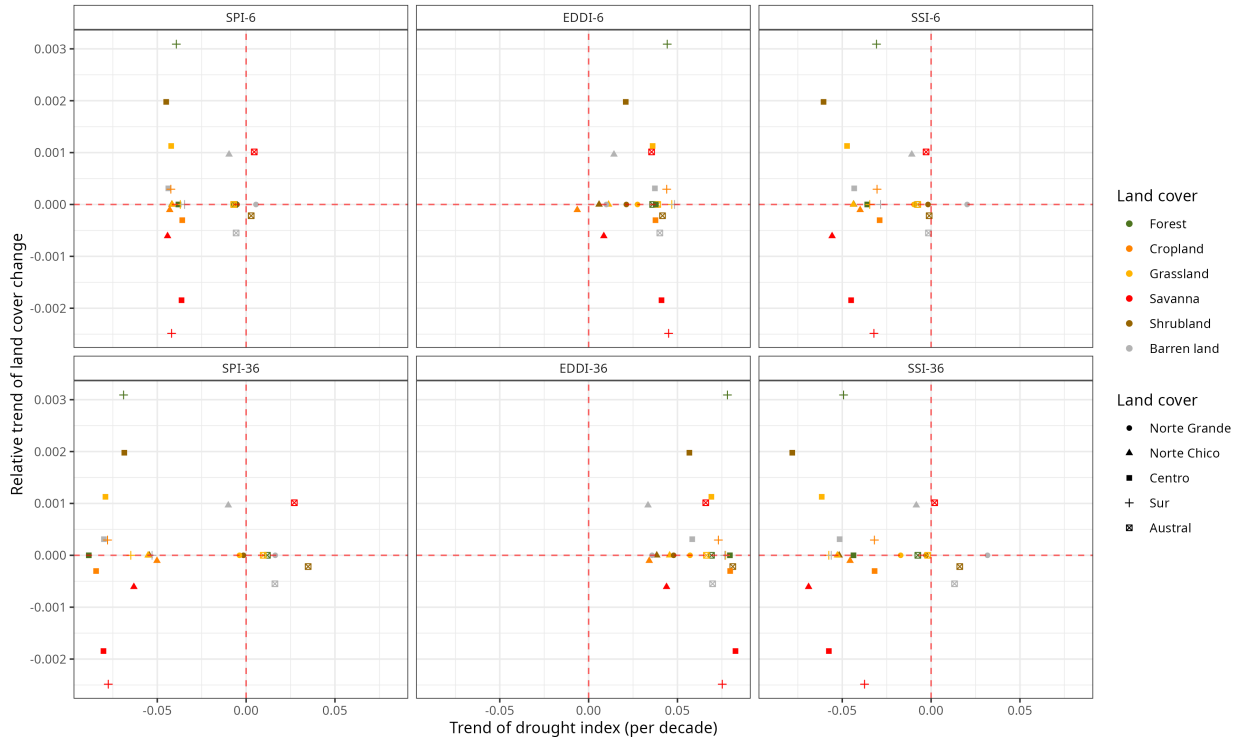


Figure 5: Relationship between the trend in land cover change (y-axis) and the trend in drought indices (x-axis) for the five macrozones. Vertical panels correspond to 1, 3, 6, 12, 24, and 36 months of the time scale by drought index. Horizontal panels show each drought index

332 We study the connection between the SPI, EDDI, and SSI drought indices and changes in land cover in  
 333 Figure 5. To do this, we compare the relative changes in land cover (in terms of the total surface area per  
 334 land cover type and macrozone) over six and thirty-six months. Figure 5 shows that the forest in the “Sur,”  
 335 shrubland and grassland in “Centro,” barren land in “Norte Chico,” and savanna in “Austral” showed an  
 336 increase in the surface of landcover associated with an increase in EDDI. Savanna in “Centro,” “Sur,” and

337 “Norte Chico” decreases with the increase in EDDI. The SPI and SSI showed similar behavior regarding  
 338 the trend in land cover type. A decrease in SPI and SSI is associated with an increase in the surface in  
 339 shrubland and grassland in “Centro,” forest in “Sur,” and barren land in “Norte Chico,” as well as a  
 340 decrease trend in savanna in “Norte Chico,” “Centro,” and “Sur.”

341 *4.3. Drought impacts on vegetation productivity within land cover*

342 *4.3.1. Trends in vegetation productivity*

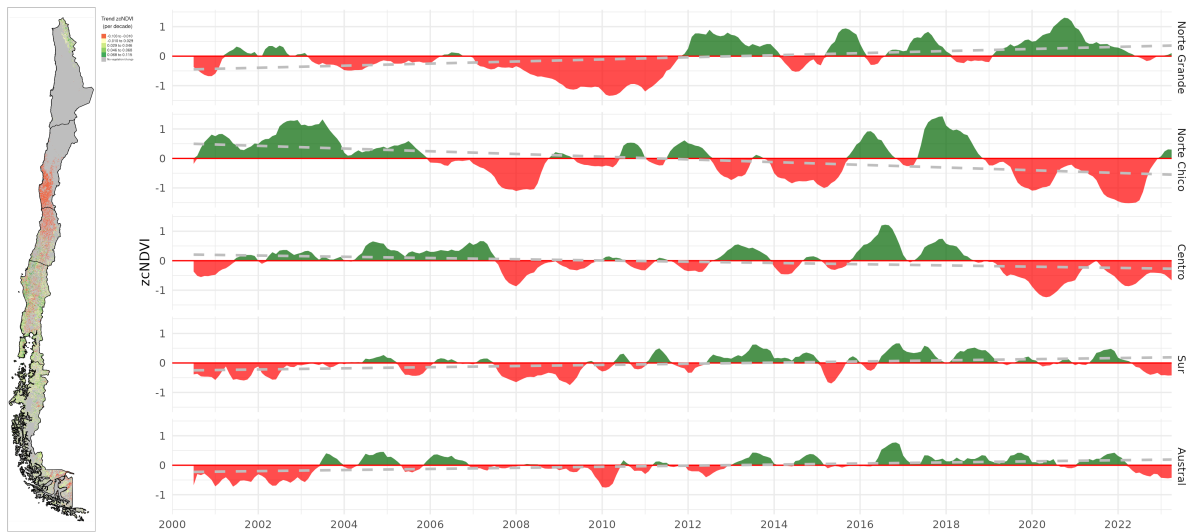


Figure 6: (a) Map of the linear trend of the index zcNDVI for 2000–2023. Greener colors indicate a positive trend; redder colors correspond to a negative trend and a decrease in vegetation productivity. Grey colors indicate either no vegetation or a change in land cover type for 2001–2022. (b) Temporal variation of zcNDVI aggregated at macrozone level within continental Chile. Each horizontal panel corresponds to a macrozone from ‘Norte Grande’ to ‘Austral’.

343 The temporal variation within the macrozones is shown in Figure 6b). There is a negative trend in “Norte  
 344 Chico” with -0.035 and “Centro” with -0.02 per decade. Vegetation reached its lowest values for 2019-2022,  
 345 with an extreme condition in early 2020 and 2022 in the “Norte Chico” and “Centro”. The “Sur” and  
 346 “Austral” show a positive trend of around 0.012 and 0.016, respectively (Figure 6).

347 In Figure 6 it is showed the spatial map of trends in zcNDVI (Figure 6a). In “Norte Grande,” vegetation  
 348 productivity, as per the z-index, exhibits a yearly increase of 0.027 for grassland and 0.032 for shrubland. In  
 349 the “Norte Chico,” savanna has the lowest trend of -0.062, cropland -0.047, shrubland -0.042, and grassland  
 350 -0.037. In “Centro,” shrubland reaches -0.07, savanna -0.031, cropland -0.024, forest -0.017, and grassland  
 351 -0.005 per decade. This decrease in productivity could be associated either with a reduction in vegetation  
 352 surface, a decrease in biomass, or browning.

353 *4.3.2. Correlation between vegetation productivity and drought indices*

354 Figure 7 shows the highest coefficient of determination ( $r^2$ , or rsq) found in the regression analysis  
 355 between zcNDVI and different drought indicators over time scales of 1, 3, 6, 12, 24, and 36 months. The  
 356 spatial variation of time scales reached per index is mostly for time scales above 12 months. In the case of  
 357 SSI, the predominant scales are 6 and 12 months. For all indices, to the north, the time scales are higher  
 358 and diminish toward the south until the south part of “Austral,” where they increase. In Figure 8, the map  
 359 of Pearson correlation values ( $r$ ) is shown. The EDDI reached correlations above 0.5 between “Norte Chico”  
 360 and “Sur.” The correlation changes from negative to positive toward the Andes Mountains and to the sea,  
 361 just as in the northern part of “Austral.” The SPI and SPEI have similar results, with the higher values in  
 362 “Norte Chico” and “Centro” being higher than 0.6. Following a similar spatial pattern as EDDI but with an

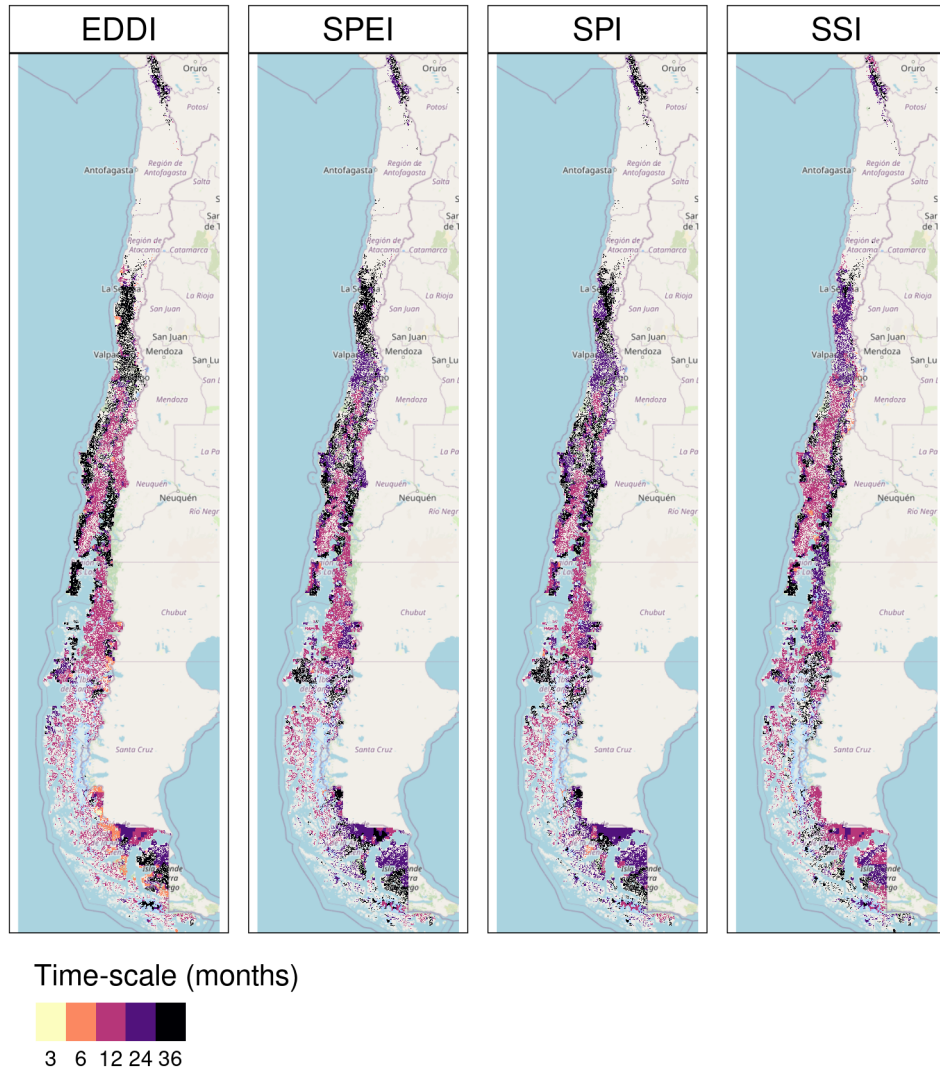


Figure 7: Time scales per drought index that reach the maximum coefficient of determination

opposite sign. The SSI showed to be the index that has a major spatial extension with a higher correlation. It has a similar correlation to SPI and SPEI for “Norte Chico” and “Sur,” but has improvements for “Sur.”

In Table 5, we aggregate per macrozone and landcover the correlation analysis presented in Figure 7 and Figure 8. According to what is shown, forests seem to be the most resistant to drought. Showing that only “Centro” is slightly ( $rsq = 0.25$ ) impacted by a 12-month soil moisture deficit (SSI-12). In the “Norte Chico” and to a lesser extent in the “Norte Grande,” it is evident that a SSI-12 with a  $rsq = 0.45$  and a decrease in water supply (SPI-36 and SPEI-24 with  $rsq = 0.28$  and  $0.34$ , respectively) have an impact on grasslands. However, this type was unaffected by soil moisture, water supply, or demand in macrozones further south. The types that show to be most affected by variation in climate conditions are shrublands, savannas, and croplands. For savannas in “Norte Chico,” the SSI-12 and SPI-24 reached an  $rsq$  of  $0.74$  and  $0.58$ , respectively. This value decreases to the south, but the SSI-12 is still the variable explaining more of the variation in vegetation productivity ( $rsq = 0.45$  in “Centro” and  $0.2$  in “Sur”). In the case of croplands, the SPEI-12, SPI-36, and SSI-12 explain between  $45\%$  and  $66\%$  of the variability in “Norte Chico.” The type of land most impacted by climatic variation was shrubland, where soil moisture explained

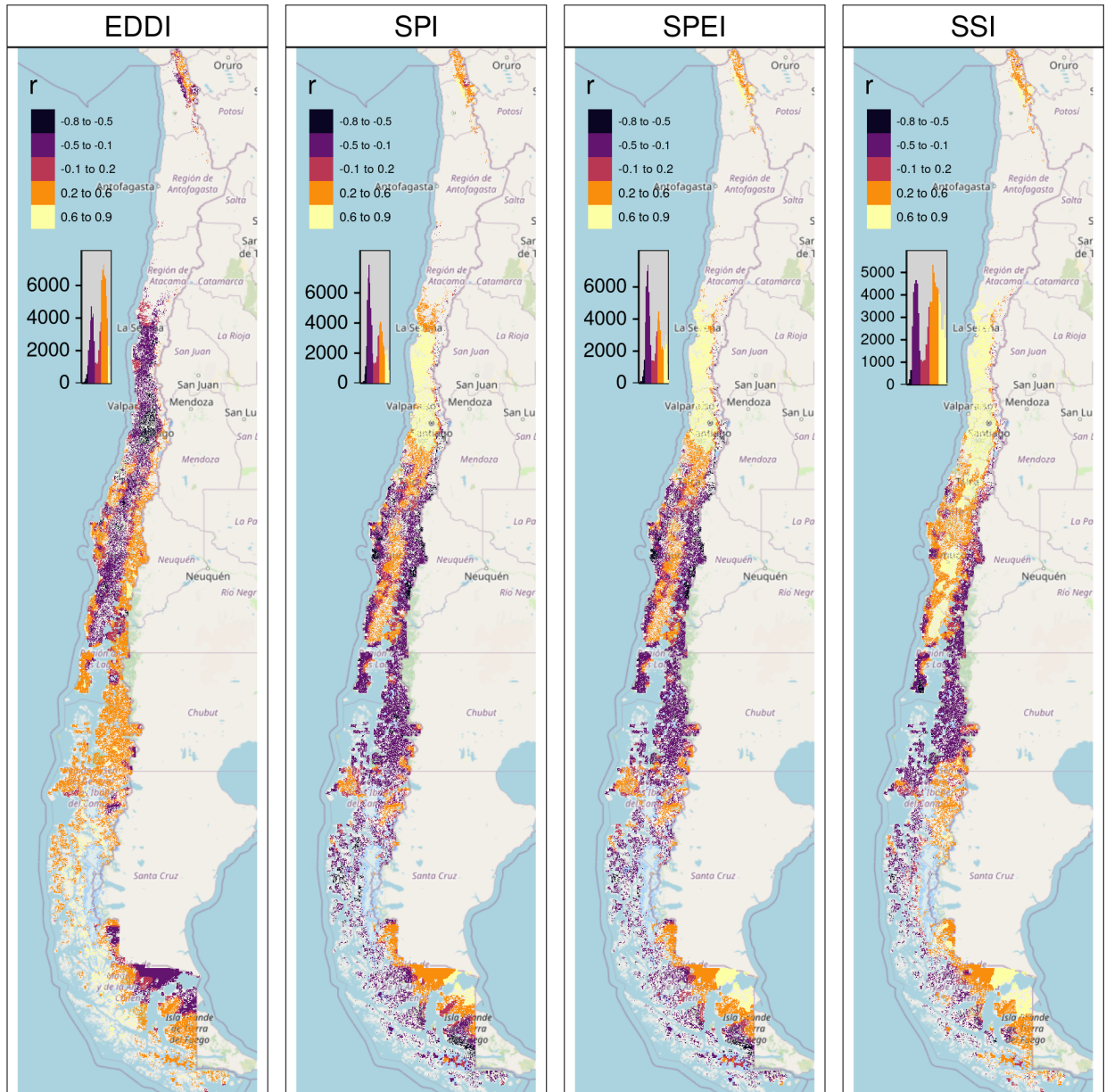


Figure 8: Pearson correlation value for the time scales and drought index that reach the maximum coefficient of determination

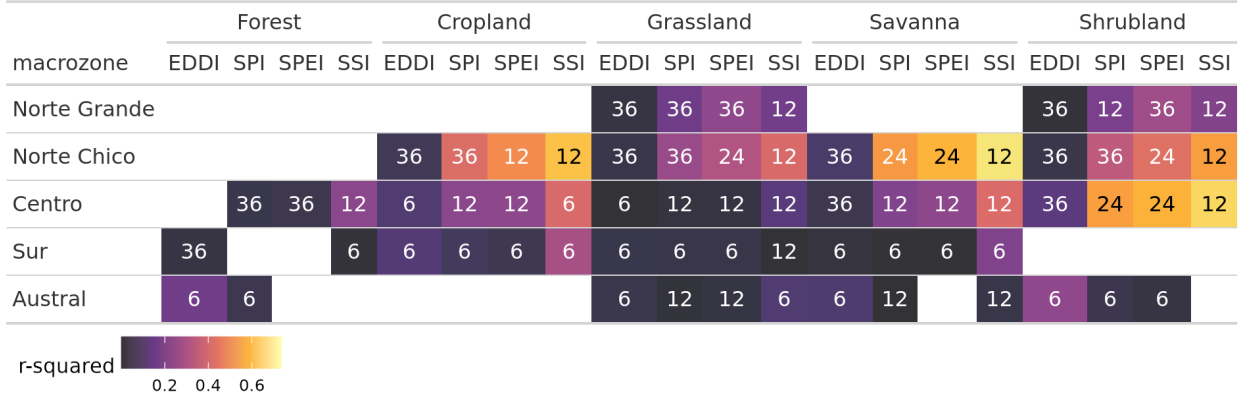
377 59% and precipitation, 37%, in “Norte Chico” and “Centro,” with SSI-12 being the most relevant variable,  
 378 then SPI-36 in “Norte Chico” and SPI-24 in “Sur.”

## 379 5. Discussion

### 380 5.1. The main drivers of drought in Chile

381 Vicente-Serrano et al. (2022), in a study at the global scale of drought trends, indicates that there have  
 382 not been significant trends in meteorological drought since 1950. Also, state that the increase in hidrological  
 383 trend in some parts of the globe (northeast Brazil and the Mediterranean region) is related to changes

Table 5: Summary per land cover macroclass and macrozone regarding the correlation between zcNDVI with the drought indices EDDI, SPI, SPEI, and SSI for time scales of 1, 3, 6, 12, 24, and 36. The numbers in each cell indicate the time scale that reached the maximum correlation for the land cover and macrozone, and the color indicates the strength of the r-squared obtained with the index and the time scale.



in land cover and specifically to the rapidly increasing irrigated area, which consequently increases water extraction. Kogan et al. (2020) analyzed the agricultural drought impact globally and in the main grain producer countries, finding that “since 1980, the Earth warming has not changed the drought area or intensity.” In our study, we took into account the variation in vegetation productivity in Chile, specifically in areas without any changes in land cover, to prevent any misleading conclusions about the increase in water demand due to land cover change. Our results show a contrasting perspective. The SPI, SPEI, and SSI (water supply) showed a decrease in trends, except for the southern part, and an increase in EDDI (water demand). The trend, positive or negative, was stronger as the time scales increased. Trends in the long term (e.g., 36 months) are evidence of how human-induced climate change is affecting Chile, which seems to be due to an intense hydrological drought resulting from the persistence of the precipitation deficit. We found that there has been a significant trend in the decline of vegetation productivity (zcNDVI) since 2000 for the north-central part of the country, which has been extreme between 2020 and 2022 and has impacted natural and cultivated land. Additionally, we demonstrated that the drought, primarily due to an increase in AED, accounts for about 30% of the changes in land cover types (excluding croplands). These changes are associated with a decrease in water demand from vegetation. Moreover, the most water-demanding type, cropland, showed a decrease in the north-central region, while barren land showed an increase. The north-central part of the country primarily experienced these changes due to a higher increase in AED. Thus, we have evidence of a significant decline in water supply and an increase in AED for the north-central part of Chile, which show to be the most relevant variables for drought conditions. Some questions arise regarding what is occurring with the cultivated land. We used the unchanged land cover to ensure that an increase in surface area is not considered in the trend analysis. For croplands, it could happen that some areas have changed the types of crops for others with higher water demand, which consequently increases water demand. However, this effect should be minor compared to the decrease in water supply and increase in water demand at this scale of analysis.

This shows that the main cause of the hydrological drought in Chile was a steady drop in water supply made worse by an increase in AED, but it seems that in zones most affected by drought, the main cause is not an increase in vegetation water demand due to an intensification of cultivated land (e.g., an increase in irrigated crops). North-central Chile has experienced a decline in vegetation productivity across land cover types, which is primarily attributable to variations in water supply and soil moisture. An increase in water demand, such as an increase in the surface area of irrigated crops, could strengthen this trend. But it is out of the scope of this study. Future work should focus on the regions where the drought has been more severe and has a high proportion of irrigated crops to get insight on the real impact of irrigation on those zones.

416    *5.2. Land cover sensitivity to drought*

417    We analyzed two main impacts of drought on land cover. First, the attribution of drought to the change  
418    in surface area per land cover type. Drought accounts for about 30% of the surface change per land cover  
419    type, with the exception of croplands. The main variables associated with these changes are the increase  
420    in AED and, in second place, the decrease in precipitation. Second, we analyzed the time series of drought  
421    indices and vegetation productivity per land cover type. In this case, the most important variables that had  
422    an impact on zcNDVI were the soil moisture deficit, followed by the precipitation deficit, and in third place,  
423    AED.

424    In a study in the Yangtze River Basin in China, [Jiang et al. \(2020\)](#) analyzed the impact of drought on  
425    vegetation using the SPEI and the Enhanced Vegetation Index (EVI). They found that cropland was more  
426    sensitive to drought than grassland, showing that cropland responds strongly to short- and medium-term  
427    drought (< SPEI-6). In our case, the SPEI-12 was the one that most impacted the croplands in “Norte  
428    Chico” and “Centro.” In general, most studies show that croplands are most sensitive to short-term drought  
429    (< SPI-6) ([Zambrano et al., 2016](#); [Potopová et al., 2015](#); [Dai et al., 2020](#); [Rhee et al., 2010](#)). Short-term  
430    precipitation deficits impact soil water, and thus less water is available for plant growth. However, we  
431    found that in “Norte Chico,” an SPI-36 and SPEI-12 had a higher impact, which are associated with  
432    hydrological drought (long-term), and in “Centro,” an SPI-12 and SPEI-12. Thus, we attribute this impact  
433    to the hydrological drought that has decreased groundwater storage ([Tau care et al., 2024](#)), which in turn  
434    is impacted by long-term deficits, and consequently, the vegetation is more dependent on groundwater. In  
435    “Sur” and “Austral,” the correlations between drought indices and vegetation productivity decrease, as do  
436    the time scales that reach the maximum r-squared. The possible reason for this is that the most resistant  
437    types, forest and grassland, predominate south of “Centro.” Also, drought episodes have been less frequent  
438    and intense. The drought episodes have had a lower impact on water availability for vegetation.

439    According to [Senf et al. \(2020\)](#), severe drought conditions in Europe are a significant cause of tree mortality.  
440    However, we discovered that forests, as the most resilient land cover class to drought, experience less variation  
441    in drought indices. Supporting this is [Fathi-Taperasht et al. \(2022\)](#), who asserts that Indian forests are the  
442    most drought-resistant and recover rapidly. Similarly, the work of [Wu et al. \(2024\)](#), who analyzed vegetation  
443    loss and recovery in response to meteorological drought in the humid subtropical Pearl River basin in China,  
444    indicates that forests showed higher drought resistance. Using Vegetation Optical Depth (VOD), kNDVI,  
445    and EVI, [Xiao et al. \(2023\)](#) tests the resistance of ecosystems and finds that ecosystems with more forests  
446    are better able to handle severe droughts than croplands. They attribute the difference to a deeper rooting  
447    depth for trees, a higher water storage capacity, and different water use strategies between forest and  
448    cropland ([Xiao et al., 2023](#)). In contrast, [Venegas-González et al. \(2023\)](#), who studied *Cryptocarya alba* and  
449    *Beilschmiedia miersii* (both from the Lauraceae family) that live in sclerophyllous forests in Chile, found  
450    that the trees’ overall growth had slowed down. This could mean that the natural dynamics of their forests  
451    have changed. They attributed it to the cumulative effects of the unprecedented drought (i.e., hydrological  
452    drought).

453    Thus, we attribute that forest to being the most resistant to drought, due to the fact that most of the species  
454    comprising it are highly resilient to water scarcity compared to the other land cover classes. Nonetheless, if  
455    we want to go deep in our analysis, we should use earth observation data that is able to capture a higher  
456    level of detail. For example, when we used MOD13A3 with a 1km spatial resolution to measure vegetation  
457    condition, it took the average condition of 1 square kilometer. Then, to use remote sensing to look at how a  
458    certain type of forest (like sclerophyllous forest) changes in response to drought on a local level, we should  
459    use operational products with higher spatial resolutions, like those from Landsat or Sentinel. This will let  
460    us do a more thorough analysis.

461    *5.3. Vegetation productivity and drought.*

462    We found that the 12-month soil moisture deficit most affects the productivity of vegetation in all land  
463    cover types along Chile. The main external factors that affect biomass production by vegetation are actual  
464    evapotranspiration and soil moisture, and the rate of ET in turn depends on the availability of water storage

465 in the root zone. Thus, soil moisture plays a key role in land carbon uptake and, consequently, in the  
466 production of biomass (Humphrey et al., 2021). Moreover, Zhang et al. (2022) indicate there is a bidirectional  
467 causality between soil moisture and vegetation productivity. Lastly, some studies have redefined agricultural  
468 drought as soil moisture drought from a hydrological perspective (Van Loon et al., 2016; Samaniego et al.,  
469 2018). Even though soil moisture is the external factor most determinant of vegetation biomass, there  
470 are multiple internal factors, such as species, physiological characteristics, and plant hydraulics, that would  
471 affect vegetation productivity. Because of that, we believe that agricultural drought, referring to the drought  
472 that impacts vegetation productivity, is the most proper term, as originally defined by Wilhite and Glantz  
473 (1985).

474 The study results showed that the soil moisture-based drought index (SSI) was better at explaining vegetation  
475 productivity across land cover macroclasses than meteorological drought indices like SPI, SPEI, and  
476 EDDI. In the early growing season and especially in irrigated rather than rainfed croplands, soil moisture  
477 has better skills than SPI and SPEI for estimating gross primary production (GPP). This according to  
478 Chatterjee et al. (2022) evaluation of the SPI and SPEI and their correlation with GPP in the CONUS.  
479 Also, Zhou et al. (2021) indicate that the monthly scaled Standardized Water Deficit Index (SWDI) can  
480 accurately show the effects of agricultural drought in most of China. Nicolai-Shaw et al. (2017) also looked  
481 at the time-lag between the SWDI and the Vegetation Condition Index (VCI). They found that there was  
482 little to no time-lag in croplands but a greater time-lag in forests.

483 In our case, there is strong spatial variability throughout Chile and between classes, mainly attributable to  
484 climate heterogeneity, hydrological status, or vegetation resistance to water scarcity. The semi-arid “Norte  
485 Chico” and the Mediterranean “Centro” were where SSI had the best performance. In Chile, medium-term  
486 deficits of 12 months are more relevant in the response of vegetation, which decreases to the south, and in the  
487 case of croplands, they seem to react in a shorter time, with six months (SSI-6) in “Centro.” This variation  
488 for croplands could be related to the fact that in “Norte Chico,” the majority of crops are irrigated, but  
489 to the south there is a higher proportion of rainfed agriculture, which is most dependent on the short-term  
490 availability of water. Rather, in the “Norte Chico,” the orchards are more dependent on the storage of water  
491 in dams of groundwater reservoirs, which are affected by long-term drought (e.g., SPI-36).

#### 492 5.4. Future outlook (to complete)

## 493 6. Conclusion

494 There is a trend toward decreasing water supply in most parts of Chile, particularly in the “Centro” and  
495 “Norte Chico” regions. The whole country showed an increase in AED. Vegetation productivity only showed  
496 a decrease in the “Norte Chico” and “Centro,” being highest for shrubland and croplands. Forest is the land  
497 cover most resistant to drought, as shown along Chile, and shrubland and cropland are the most sensitive.

498 A soil moisture deficit of 12 months (SSI-12) is highly correlated with vegetation productivity for the land  
499 cover classes of shrubland, savannas, croplands, and forest in “Norte Chico” and “Centro.” For the southern  
500 part of the country with humid conditions, the correlation with SSI decreases. Soil moisture overcomes  
501 the capacity to explain vegetation productivity over the supply and demand drought indices in the entire  
502 territory.

503 The variation in vegetation productivity appears to be associated with climate variation rather than an-  
504 thropogenic factors (e.g., an increase in water demand by irrigated crops). Even though switching to more  
505 demanding crops on the land could increase the impact of drought on vegetation, this would need to be  
506 more thoroughly investigated, for instance at the watershed level.

507 The results of this study could help in the development of a robust forecasting system for land cover classes  
508 in Chile, helping to improve preparedness for climate change impacts on vegetation.

- 509 **References**
- 510 Abramowitz, M., Stegun, I.A., 1968. Handbook of mathematical functions with formulas, graphs, and mathematical tables. volume 55. US Government printing office.
- 511 Aceituno, P., Boisier, J.P., Garreaud, R., Rondanelli, R., Rutllant, J.A., 2021. Climate and Weather in Chile, in: Fernández, B., Gironás, J. (Eds.), Water Resources of Chile. Springer International Publishing, Cham. volume 8, pp. 7–29. URL: [http://link.springer.com/10.1007/978-3-030-56901-3\\_2](http://link.springer.com/10.1007/978-3-030-56901-3_2).
- 512 AghaKouchak, A., 2014. A baseline probabilistic drought forecasting framework using standardized soil moisture index: application to the 2012 United States drought. *Hydrology and Earth System Sciences* 18, 2485–2492. URL: <https://hess.copernicus.org/articles/18/2485/2014/>, doi:10.5194/hess-18-2485-2014.
- 513 AghaKouchak, A., Mirchi, A., Madani, K., Di Baldassarre, G., Nazemi, A., Alborzi, A., Anjileli, H., Azarderakhsh, M., Chiang, F., Hassanzadeh, E., Huning, L.S., Mallakpour, I., Martinez, A., Mazdiyasni, O., Moftakhari, H., Norouzi, H., Sadegh, M., Sadeqi, D., Van Loon, A.F., Wanders, N., 2021. Anthropogenic Drought: Definition, Challenges, and Opportunities. *Reviews of Geophysics* 59, e2019RG000683. URL: <https://agupubs.onlinelibrary.wiley.com/doi/10.1029/2019RG000683>, doi:10.1029/2019RG000683.
- 514 Akinyemi, F.O., 2021. Vegetation Trends, Drought Severity and Land Use-Land Cover Change during the Growing Season in Semi-Arid Contexts. *Remote Sensing* 2021, Vol. 13, Page 836 13, 836. URL: <https://www.mdpi.com/2072-4292/13/5/836/htm>, doi:10.3390/RS13050836. publisher: Multidisciplinary Digital Publishing Institute.
- 515 Bakker, K., 2012. Water Security: Research Challenges and Opportunities. *Science* 337, 914–915. URL: <https://www.science.org/doi/10.1126/science.1226337>, doi:10.1126/science.1226337.
- 516 Beck, H.E., McVicar, T.R., Vergopolan, N., Berg, A., Lutsko, N.J., Dufour, A., Zeng, Z., Jiang, X., van Dijk, A.I.J.M., Miralles, D.G., 2023. High-resolution (1 km) Köppen-Geiger maps for 1901–2099 based on constrained CMIP6 projections. *Scientific Data* 10. URL: <http://dx.doi.org/10.1038/s41597-023-02549-6>, doi:10.1038/s41597-023-02549-6.
- 517 Beguería, S., Vicente-Serrano, S.M., 2023. SPEI: Calculation of the Standardized Precipitation-Evapotranspiration Index. URL: <https://CRAN.R-project.org/package=SPEI>.
- 518 Boisier, J.P., Alvarez-Garreton, C., Cordero, R.R., Damiani, A., Gallardo, L., Garreaud, R.D., Lambert, F., Ramallo, C., Rojas, M., Rondanelli, R., 2018. Anthropogenic drying in central-southern Chile evidenced by long-term observations and climate model simulations. *Elementa* 6, 74. URL: <https://www.elementascience.org/article/10.1525/elementa.328/>, doi:10.1525/elementa.328.
- 519 Calvin, K., Dasgupta, D., Krinner, G., Mukherji, A., Thorne, P.W., Trisos, C., Romero, J., Aldunce, P., Barrett, K., Blanco, G., Cheung, W.W., Connors, S., Denton, F., Diongue-Niang, A., Dodman, D., Garschagen, M., Geden, O., Hayward, B., Jones, C., Jotzo, F., Krug, T., Lasco, R., Lee, Y.Y., Masson-Delmotte, V., Meinshausen, M., Mintenbeck, K., Mokssit, A., Otto, F.E., Pathak, M., Pirani, A., Poloczanska, E., Pörtner, H.O., Revi, A., Roberts, D.C., Roy, J., Ruane, A.C., Skea, J., Shukla, P.R., Slade, R., Slangen, A., Sokona, Y., Sörensson, A.A., Tignor, M., Van Vuuren, D., Wei, Y.M., Winkler, H., Zhai, P., Zommers, Z., Hourcade, J.C., Johnson, F.X., Pachauri, S., Simpson, N.P., Singh, C., Thomas, A., Totin, E., Arias, P., Bustamante, M., Elgizouli, I., Flato, G., Howden, M., Méndez-Vallejo, C., Pereira, J.J., Pichs-Madruga, R., Rose, S.K., Saheb, Y., Sánchez Rodríguez, R., Ürge Vorsatz, D., Xiao, C., Yassa, N., Alegría, A., Armour, K., Bednar-Friedl, B., Blok, K., Cissé, G., Dentener, F., Eriksen, S., Fischer, E., Garner, G., Guiavarch, C., Haasnoot, M., Hansen, G., Hauser, M., Hawkins, E., Hermans, T., Kopp, R., Leprince-Ringuet, N., Lewis, J., Ley, D., Ludden, C., Niamir, L., Nicholls, Z., Some, S., Szopa, S., Trewhin, B., Van Der Wijst, K.I., Winter, G., Witting, M., Birt, A., Ha, M., Romero, J., Kim, J., Haites, E.F., Jung, Y., Stavins, R., Birt, A., Ha, M., Orendain, D.J.A., Ignon, L., Park, S., Park, Y., Reisinger, A., Cammaramo, D., Fischlin, A., Fuglestvedt, J.S., Hansen, G., Ludden, C., Masson-Delmotte, V., Matthews, J.R., Mintenbeck, K., Pirani, A., Poloczanska, E., Leprince-Ringuet, N., Péan, C., 2023. IPCC, 2023: Climate Change 2023: Synthesis Report. Contribution of Working Groups I, II and III to the Sixth Assessment Report of the Intergovernmental Panel on Climate Change [Core Writing Team, H. Lee and J. Romero (eds.)]. IPCC, Geneva, Switzerland. Technical Report. Intergovernmental Panel on Climate Change (IPCC). URL: <https://www.ipcc.ch/report/ar6/syr/>.
- 520 Camps-Valls, G., Campos-Taberner, M., Moreno-Martínez, , Walther, S., Duveiller, G., Cescatti, A., Mahecha, M.D., Muñoz-Marí, J., García-Haro, F.J., Guanter, L., Jung, M., Gamon, J.A., Reichstein, M., Running, S.W., 2021. A unified vegetation index for quantifying the terrestrial biosphere. *Science Advances* 7, eabc7447. URL: <https://www.science.org/doi/10.1126/sciadv.abc7447>, doi:10.1126/sciadv.abc7447.
- 521 Chamlng, M., Bera, B., 2020. Spatio-temporal Patterns of Land Use/Land Cover Change in the Bhutan–Bengal Foothill Region Between 1987 and 2019: Study Towards Geospatial Applications and Policy Making. *Earth Systems and Environment* 4, 117–130. URL: <http://link.springer.com/10.1007/s41748-020-00150-0>, doi:10.1007/s41748-020-00150-0.
- 522 Chatterjee, S., Desai, A.R., Zhu, J., Townsend, P.A., Huang, J., 2022. Soil moisture as an essential component for delineating and forecasting agricultural rather than meteorological drought. *Remote Sensing of Environment* 269, 112833. URL: <https://linkinghub.elsevier.com/retrieve/pii/S0034425721005538>, doi:10.1016/j.rse.2021.112833.
- 523 Chen, J., Shao, Z., Huang, X., Zhuang, Q., Dang, C., Cai, B., Zheng, X., Ding, Q., 2022. Assessing the impact of drought-land cover change on global vegetation greenness and productivity. *Science of The Total Environment* 852, 158499. URL: <https://linkinghub.elsevier.com/retrieve/pii/S004896972205598X>, doi:10.1016/j.scitotenv.2022.158499.
- 524 Crausbay, S.D., Ramirez, A.R., Carter, S.L., Cross, M.S., Hall, K.R., Bathke, D.J., Betancourt, J.L., Colt, S., Cravens, A.E., Dalton, M.S., Dunham, J.B., Hay, L.E., Hayes, M.J., McEvoy, J., McNutt, C.A., Moritz, M.A., Nislow, K.H., Raheem, N., Sanford, T., 2017. Defining Ecological Drought for the Twenty-First Century. *Bulletin of the American Meteorological Society* 98, 2543–2550. URL: <https://journals.ametsoc.org/view/journals/bams/98/12/bams-d-16-0292.1.xml>, doi:10.1175/BAMS-D-16-0292.1. publisher: American Meteorological Society.
- 525 Dai, M., Huang, S., Huang, Q., Leng, G., Guo, Y., Wang, L., Fang, W., Li, P., Zheng, X., 2020. Assessing agricultural drought

- 573 risk and its dynamic evolution characteristics. Agricultural Water Management 231, 106003. URL: <https://linkinghub.elsevier.com/retrieve/pii/S0378377419316531>, doi:[10.1016/j.agwat.2020.106003](https://doi.org/10.1016/j.agwat.2020.106003).
- 574 Didan, K., 2015. MOD13Q1 MODIS/Terra Vegetation Indices 16-Day L3 Global 250m SIN Grid V006. Technical Report.
- 575 NASA EOSDIS Land Processes DAAC. doi:<http://dx.doi.org/10.5067/MODIS/MOD13Q1.006>.
- 576 Farahmand, A., AghaKouchak, A., 2015. A generalized framework for deriving nonparametric standardized drought indicators.
- 577 Advances in Water Resources 76, 140–145. URL: <https://linkinghub.elsevier.com/retrieve/pii/S0309170814002322>, doi:[10.1016/j.advwatres.2014.11.012](https://doi.org/10.1016/j.advwatres.2014.11.012).
- 578 Fathi-Taperasht, A., Shafizadeh-Moghadam, H., Minaei, M., Xu, T., 2022. Influence of drought duration and severity on
- 579 drought recovery period for different land cover types: evaluation using MODIS-based indices. Ecological Indicators 141,
- 580 109146. URL: <https://linkinghub.elsevier.com/retrieve/pii/S1470160X22006185>, doi:[10.1016/j.ecolind.2022.109146](https://doi.org/10.1016/j.ecolind.2022.109146).
- 581 Ford, T.W., Otkin, J.A., Quiring, S.M., Lisonbee, J., Woloszyn, M., Wang, J., Zhong, Y., 2023. Flash Drought Indicator
- 582 Intercomparison in the United States. Journal of Applied Meteorology and Climatology 62, 1713–1730. URL: <https://journals.ametsoc.org/view/journals/apme/62/12/JAMC-D-23-0081.1.xml>, doi:[10.1175/JAMC-D-23-0081.1](https://doi.org/10.1175/JAMC-D-23-0081.1).
- 583 Fuentes, I., Fuster, R., Avilés, D., Vervoort, W., 2021. Water scarcity in central Chile: the effect of climate and land cover
- 584 changes on hydrologic resources. Hydrological Sciences Journal 66, 1028–1044. URL: <https://www.tandfonline.com/doi/full/10.1080/02626667.2021.1903475>, doi:[10.1080/02626667.2021.1903475](https://doi.org/10.1080/02626667.2021.1903475).
- 585 Garreaud, R., Alvarez-Garreton, C., Barichivich, J., Boisier, J.P., Christie, D., Galleguillos, M., LeQuesne, C., McPhee, J.,
- 586 Zambrano-Bigiarini, M., 2017. The 2010–2015 mega drought in Central Chile: Impacts on regional hydroclimate and
- 587 vegetation. Hydrology and Earth System Sciences Discussions 2017, 1–37. URL: <http://www.hydrol-earth-syst-sci-discuss.net/hess-2017-191/>, doi:[10.5194/hess-2017-191](https://doi.org/10.5194/hess-2017-191).
- 588 Garreaud, R.D., 2009. The Andes climate and weather. Advances in Geosciences 22, 3–11. URL: <https://adgeo.copernicus.org/articles/22/3/2009/>, doi:[10.5194/adgeo-22-3-2009](https://doi.org/10.5194/adgeo-22-3-2009).
- 589 Gebrechorkos, S.H., Peng, J., Dyer, E., Miralles, D.G., Vicente-Serrano, S.M., Funk, C., Beck, H.E., Asfaw, D.T., Singer, M.B.,
- 590 Dadson, S.J., 2023. Global high-resolution drought indices for 1981–2022. Earth System Science Data 15, 5449–5466. URL:
- 591 <https://essd.copernicus.org/articles/15/5449/2023/>, doi:[10.5194/essd-15-5449-2023](https://doi.org/10.5194/essd-15-5449-2023).
- 592 Hao, Z., AghaKouchak, A., 2013. Multivariate Standardized Drought Index: A parametric multi-index model. Advances in Water
- 593 Resources 57, 12–18. URL: <https://linkinghub.elsevier.com/retrieve/pii/S0309170813000493>, doi:[10.1016/j.advwatres.2013.03.009](https://doi.org/10.1016/j.advwatres.2013.03.009).
- 594 Hargreaves, G.H., 1994. Defining and Using Reference Evapotranspiration. Journal of Irrigation and Drainage Engineering 120,
- 595 1132–1139. URL: <https://ascelibrary.org/doi/10.1061/%28ASCE%290733-9437%281994%29120%3A6%281132%29>, doi:[10.1061/\(ASCE\)0733-9437\(1994\)120:6\(1132\)](https://doi.org/10.1061/(ASCE)0733-9437(1994)120:6(1132)).
- 596 Hargreaves, G.H., Samani, Z.A., 1985. Reference crop evapotranspiration from temperature. Applied engineering in agriculture
- 597 1, 96–99.
- 598 Heim, R.R., 2002. A Review of Twentieth-Century Drought Indices Used in the United States. Bulletin of the American
- 599 Meteorological Society 83, 1149–1166. URL: <https://journals.ametsoc.org/doi/10.1175/1520-0477-83.8.1149>, doi:[10.1175/1520-0477-83.8.1149](https://doi.org/10.1175/1520-0477-83.8.1149).
- 600 Helman, D., Mussery, A., Lensky, I.M., Leu, S., 2014. Detecting changes in biomass productivity in a different land management
- 601 regimes in drylands using satellite-derived vegetation index. Soil Use and Management 30, 32–39. URL: <https://bsssjournals.onlinelibrary.wiley.com/doi/10.1111/sum.12099>, doi:[10.1111/sum.12099](https://doi.org/10.1111/sum.12099).
- 602 Hijmans, R.J., 2023. terra: Spatial Data Analysis. URL: <https://CRAN.R-project.org/package=terra>.
- 603 Hobbins, M.T., Wood, A., McEvoy, D.J., Huntington, J.L., Morton, C., Anderson, M., Hain, C., 2016. The Evaporative Demand
- 604 Drought Index. Part I: Linking Drought Evolution to Variations in Evaporative Demand. Journal of Hydrometeorology 17,
- 605 1745–1761. URL: <https://journals.ametsoc.org/doi/10.1175/JHM-D-15-0121.1>, doi:[10.1175/JHM-D-15-0121.1](https://doi.org/10.1175/JHM-D-15-0121.1).
- 606 Homer, C., Dewitz, J., Jin, S., Xian, G., Costello, C., Danielson, P., Gass, L., Funk, M., Wickham, J., Stehman, S., Auch, R.,
- 607 Riitters, K., 2020. Conterminous United States land cover change patterns 2001–2016 from the 2016 National Land Cover
- 608 Database. ISPRS Journal of Photogrammetry and Remote Sensing 162, 184–199. URL: <https://linkinghub.elsevier.com/retrieve/pii/S0924271620300587>, doi:[10.1016/j.isprsjprs.2020.02.019](https://doi.org/10.1016/j.isprsjprs.2020.02.019).
- 609 Hufkens, K., Stauffer, R., Campitelli, E., 2019. The ecwmfr package: an interface to ECMWF API endpoints. URL: <https://bluegreen-labs.github.io/ecmwfr/>.
- 610 Humphrey, V., Berg, A., Ciais, P., Gentine, P., Jung, M., Reichstein, M., Seneviratne, S.I., Frankenberg, C., 2021. Soil
- 611 moisture–atmosphere feedback dominates land carbon uptake variability. Nature 592, 65–69. URL: <https://www.nature.com/articles/s41586-021-03325-5>, doi:[10.1038/s41586-021-03325-5](https://doi.org/10.1038/s41586-021-03325-5).
- 612 IPCC, 2013. Climate Change 2013: The Physical Science Basis. Contribution of Working Group I to the Fifth Assessment
- 613 Report of the Intergovernmental Panel on Climate Change. Cambridge University Press, Cambridge, UK; New York, USA.
- 614 URL: [www.climatechange2013.org](http://www.climatechange2013.org), doi:[10.1017/CBO9781107415324](https://doi.org/10.1017/CBO9781107415324).
- 615 Jiang, W., Wang, L., Feng, L., Zhang, M., Yao, R., 2020. Drought characteristics and its impact on changes in surface
- 616 vegetation from 1981 to 2015 in the Yangtze River Basin, China. International Journal of Climatology 40, 3380–3397. URL:
- 617 <https://rmets.onlinelibrary.wiley.com/doi/10.1002/joc.6403>, doi:[10.1002/joc.6403](https://doi.org/10.1002/joc.6403).
- 618 Kendall, M., 1975. Rank correlation methods (4th ed. 2d impression). Griffin.
- 619 Kogan, F., Guo, W., Yang, W., 2020. Near 40-year drought trend during 1981–2019 earth warming and food security. Geomatics, Natural Hazards and Risk 11, 469–490. URL: <https://www.tandfonline.com/doi/full/10.1080/19475705.2020.1730452>, doi:[10.1080/19475705.2020.1730452](https://doi.org/10.1080/19475705.2020.1730452).
- 620 Kuhn, M., Wickham, H., 2020. Tidymodels: a collection of packages for modeling and machine learning using tidyverse
- 621 principles. URL: <https://www.tidymodels.org>.
- 622 Laimighofer, J., Laaha, G., 2022. How standard are standardized drought indices? Uncertainty components for the SPI

- 638 & SPEI case. *Journal of Hydrology* 613, 128385. URL: <https://linkinghub.elsevier.com/retrieve/pii/S0022169422009544>,  
 639 doi:[10.1016/j.jhydrol.2022.128385](https://doi.org/10.1016/j.jhydrol.2022.128385).
- 640 Li, H., Choy, S., Zaminpardaz, S., Wang, X., Liang, H., Zhang, K., 2024. Flash drought monitoring using diurnal-provided  
 641 evaporative demand drought index. *Journal of Hydrology* 633, 130961. URL: <https://linkinghub.elsevier.com/retrieve/pii/>  
 642 [S002216942400355X](https://doi.org/10.1016/j.jhydrol.2024.130961), doi:[10.1016/j.jhydrol.2024.130961](https://doi.org/10.1016/j.jhydrol.2024.130961).
- 643 Li, W., Migliavacca, M., Forkel, M., Denissen, J.M.C., Reichstein, M., Yang, H., Duveiller, G., Weber, U., Orth, R., 2022.  
 644 Widespread increasing vegetation sensitivity to soil moisture. *Nature Communications* 13, 3959. URL: <https://www.nature.com/articles/s41467-022-31667-9>, doi:[10.1038/s41467-022-31667-9](https://doi.org/10.1038/s41467-022-31667-9).
- 645 Liu, X., Yu, S., Yang, Z., Dong, J., Peng, J., 2024. The first global multi-timescale daily SPEI dataset from 1982 to 2021.  
 646 *Scientific Data* 11, 223. URL: <https://www.nature.com/articles/s41597-024-03047-z>, doi:[10.1038/s41597-024-03047-z](https://doi.org/10.1038/s41597-024-03047-z).
- 647 Luebert, F., Pliscoff, P., 2022. The vegetation of Chile and the EcoVeg approach in the context of the International Vegetation  
 648 Classification project. *Vegetation Classification and Survey* 3, 15–28. URL: <https://vcs.pensoft.net/article/67893/>, doi:[10.3897/vcs.67893](https://doi.org/10.3897/vcs.67893).
- 649 Luo, L., Apps, D., Arcand, S., Xu, H., Pan, M., Hoerling, M., 2017. Contribution of temperature and precipitation anomalies to  
 650 the California drought during 2012–2015. *Geophysical Research Letters* 44, 3184–3192. URL: <https://agupubs.onlinelibrary.wiley.com/doi/10.1002/2016GL072027>, doi:[10.1002/2016GL072027](https://doi.org/10.1002/2016GL072027).
- 651 Luyssaert, S., Jammet, M., Stoy, P.C., Estel, S., Pongratz, J., Ceschia, E., Churkina, G., Don, A., Erb, K., Ferlicqo, M.,  
 652 Gielen, B., Grünwald, T., Houghton, R.A., Klumpp, K., Knohl, A., Kolb, T., Kuemmerle, T., Laurila, T., Lohila, A.,  
 653 Loustau, D., McGrath, M.J., Meyfroidt, P., Moors, E.J., Naudts, K., Novick, K., Otto, J., Pilegaard, K., Pio, C.A., Rambal,  
 654 S., Rebmann, C., Ryder, J., Suyker, A.E., Varlagin, A., Wattenbach, M., Dolman, A.J., 2014. Land management and  
 655 land-cover change have impacts of similar magnitude on surface temperature. *Nature Climate Change* 4, 389–393. URL:  
 656 <https://www.nature.com/articles/nclimate2196>, doi:[10.1038/nclimate2196](https://doi.org/10.1038/nclimate2196).
- 657 Masson-Delmotte, V., P.Z.A.P.S.L.C.C.P.S.B.N.C.Y.C.L.G.M.I.G.M.H.K.L.E.L.J.B.R.M.T.K.M.T.W.O.Y.R.Y.a.B.Z.e., 2021.  
 658 IPCC, 2021: Climate Change 2021: The Physical Science Basis. Contribution of Working Group I to the Sixth Assessment  
 659 Report of the Intergovernmental Panel on Climate Change. Technical Report. URL: <https://www.ipcc.ch/>. publication  
 660 Title: Cambridge University Press. In Press.
- 661 McEvoy, D.J., Huntington, J.L., Hobbins, M.T., Wood, A., Morton, C., Anderson, M., Hain, C., 2016. The Evaporative Demand  
 662 Drought Index. Part II: CONUS-Wide Assessment against Common Drought Indicators. *Journal of Hydrometeorology* 17,  
 663 1763–1779. URL: <http://journals.ametsoc.org/doi/10.1175/JHM-D-15-0122.1>, doi:[10.1175/JHM-D-15-0122.1](https://doi.org/10.1175/JHM-D-15-0122.1).
- 664 Meroni, M., Rembold, F., Fasbender, D., Vrieling, A., 2017. Evaluation of the Standardized Precipitation Index as an early  
 665 predictor of seasonal vegetation production anomalies in the Sahel. *Remote Sensing Letters* 8, 301–310. URL: <http://www.tandfonline.com/doi/abs/10.1080/2150704X.2016.1264020>, doi:[10.1080/2150704X.2016.1264020](https://doi.org/10.1080/2150704X.2016.1264020).
- 666 Miranda, A., Lara, A., Altamirano, A., Di Bella, C., González, M.E., Julio Camarero, J., 2020. Forest browning trends in  
 667 response to drought in a highly threatened mediterranean landscape of South America. *Ecological Indicators* 115, 106401.  
 668 URL: <https://linkinghub.elsevier.com/retrieve/pii/S1470160X20303381>, doi:[10.1016/j.ecolind.2020.106401](https://doi.org/10.1016/j.ecolind.2020.106401).
- 669 Muñoz-Sabater, J., Dutra, E., Agustí-Panareda, A., Albergel, C., Arduini, G., Balsamo, G., Boussetta, S., Choulga, M.,  
 670 Harrigan, S., Hersbach, H., Martens, B., Miralles, D.G., Piles, M., Rodríguez-Fernández, N.J., Zsoter, E., Buontempo, C.,  
 671 Thépaut, J.N., 2021. ERA5-Land: a state-of-the-art global reanalysis dataset for land applications. *Earth System Science  
 672 Data* 13, 4349–4383. URL: <https://essd.copernicus.org/articles/13/4349/2021/>, doi:[10.5194/essd-13-4349-2021](https://doi.org/10.5194/essd-13-4349-2021).
- 673 Narasimhan, B., Srinivasan, R., 2005. Development and evaluation of Soil Moisture Deficit Index (SMDI) and Evapotranspi-  
 674 ration Deficit Index (ETDI) for agricultural drought monitoring. *Agricultural and Forest Meteorology* 133, 69–88. URL:  
 675 <https://linkinghub.elsevier.com/retrieve/pii/S0168192305001565>, doi:[10.1016/j.agrformet.2005.07.012](https://doi.org/10.1016/j.agrformet.2005.07.012).
- 676 Nicolai-Shaw, N., Zscheischler, J., Hirschi, M., Gudmundsson, L., Seneviratne, S.I., 2017. A drought event composite analysis  
 677 using satellite remote-sensing based soil moisture. *Remote Sensing of Environment* 203, 216–225. URL: <https://linkinghub.elsevier.com/retrieve/pii/S0034425717302729>, doi:[10.1016/j.rse.2017.06.014](https://doi.org/10.1016/j.rse.2017.06.014).
- 678 Noguera, I., Vicente-Serrano, S.M., Domínguez-Castro, F., 2022. The Rise of Atmospheric Evaporative Demand Is Increasing  
 679 Flash Droughts in Spain During the Warm Season. *Geophysical Research Letters* 49, e2021GL097703. URL: <https://agupubs.onlinelibrary.wiley.com/doi/10.1029/2021GL097703>, doi:[10.1029/2021GL097703](https://doi.org/10.1029/2021GL097703).
- 680 Paruelo, J.M., Texeira, M., Staiano, L., Mastrángelo, M., Amdan, L., Gallego, F., 2016. An integrative index of Ecosystem  
 681 Services provision based on remotely sensed data. *Ecological Indicators* 71, 145–154. URL: <https://www.sciencedirect.com/science/article/pii/S1470160X16303843>, doi:[10.1016/j.ecolind.2016.06.054](https://doi.org/10.1016/j.ecolind.2016.06.054). publisher: Elsevier.
- 682 Pebesma, E., 2018. Simple Features for R: Standardized Support for Spatial Vector Data. *The R Journal* 10, 439–446. URL:  
 683 <https://doi.org/10.32614/RJ-2018-009>, doi:[10.32614/RJ-2018-009](https://doi.org/10.32614/RJ-2018-009).
- 684 Pebesma, E., Bivand, R., 2023. Spatial Data Science: With applications in R. Chapman and Hall/CRC, London. URL:  
 685 <https://r-spatial.org/book/>.
- 686 Peng, D., Zhang, B., Wu, C., Huete, A.R., Gonsamo, A., Lei, L., Ponce-Campos, G.E., Liu, X., Wu, Y., 2017. Country-level  
 687 net primary production distribution and response to drought and land cover change. *Science of The Total Environment* 574,  
 688 65–77. URL: <https://linkinghub.elsevier.com/retrieve/pii/S0048969716319507>, doi:[10.1016/j.scitotenv.2016.09.033](https://doi.org/10.1016/j.scitotenv.2016.09.033).
- 689 Pitman, A.J., De Noblet-Ducoudré, N., Avila, F.B., Alexander, L.V., Boisier, J.P., Brovkin, V., Delire, C., Cruz, F., Donat,  
 690 M.G., Gayler, V., Van Den Hurk, B., Reick, C., Volodire, A., 2012. Effects of land cover change on temperature and  
 691 rainfall extremes in multi-model ensemble simulations. *Earth System Dynamics* 3, 213–231. URL: <https://esd.copernicus.org/articles/3/213/2012/>, doi:[10.5194/esd-3-213-2012](https://doi.org/10.5194/esd-3-213-2012).
- 692 Potopová, V., Stepánek, P., Mozný, M., Türkott, L., Soukup, J., 2015. Performance of the standarised precipitation evapotran-  
 693 spiration index at various lags for agricultural drought risk assessment in the {C}zech {R}epublic. *Agricultural and Forest  
 694 Meteorology* 202, 26–38.

- 703 R Core Team, 2023. R: A Language and Environment for Statistical Computing. R Foundation for Statistical Computing,  
 704 Vienna, Austria. URL: <https://www.R-project.org/>.
- 705 Rhee, J., Im, J., Carbone, G.J., 2010. Monitoring agricultural drought for arid and humid regions using multi-sensor remote  
 706 sensing data. *Remote Sensing of Environment* 114, 2875–2887. URL: <http://www.sciencedirect.com/science/article/pii/S003442571000221X>, doi:[10.1016/j.rse.2010.07.005](https://doi.org/10.1016/j.rse.2010.07.005).
- 707 Samaniego, L., Thober, S., Kumar, R., Wanders, N., Rakovec, O., Pan, M., Zink, M., Sheffield, J., Wood, E.F., Marx, A.,  
 708 2018. Anthropogenic warming exacerbates European soil moisture droughts. *Nature Climate Change* 8, 421–426. URL:  
 709 <https://www.nature.com/articles/s41558-018-0138-5>, doi:[10.1038/s41558-018-0138-5](https://doi.org/10.1038/s41558-018-0138-5).
- 710 Sen, P.K., 1968. Estimates of the Regression Coefficient Based on Kendall's Tau. *Journal of the American Statistical Association*  
 711 63, 1379–1389. URL: <http://www.tandfonline.com/doi/abs/10.1080/01621459.1968.10480934>, doi:[10.1080/01621459.1968.10480934](https://doi.org/10.1080/01621459.1968.10480934).
- 712 Senf, C., Buras, A., Zang, C.S., Rammig, A., Seidl, R., 2020. Excess forest mortality is consistently linked to drought  
 713 across Europe. *Nature Communications* 11, 6200. URL: <https://www.nature.com/articles/s41467-020-19924-1>, doi:[10.1038/s41467-020-19924-1](https://doi.org/10.1038/s41467-020-19924-1).
- 714 Slette, I.J., Post, A.K., Awad, M., Even, T., Punzalan, A., Williams, S., Smith, M.D., Knapp, A.K., 2019. How ecologists  
 715 define drought, and why we should do better. *Global Change Biology* 25, 3193–3200. URL: <https://onlinelibrary.wiley.com/doi/10.1111/gcb.14747>, doi:[10.1111/gcb.14747](https://doi.org/10.1111/gcb.14747).
- 716 Song, X.P., Hansen, M.C., Stehman, S.V., Potapov, P.V., Tyukavina, A., Vermote, E.F., Townshend, J.R., 2018. Global land  
 717 change from 1982 to 2016. *Nature* 560, 639–643. URL: <https://www.nature.com/articles/s41586-018-0411-9>, doi:[10.1038/s41586-018-0411-9](https://doi.org/10.1038/s41586-018-0411-9).
- 718 Souza, A.G.S.S., Ribeiro Neto, A., Souza, L.L.D., 2021. Soil moisture-based index for agricultural drought assessment: SMADI  
 719 application in Pernambuco State-Brazil. *Remote Sensing of Environment* 252, 112124. URL: <https://linkinghub.elsevier.com/retrieve/pii/S0034425720304971>, doi:[10.1016/j.rse.2020.112124](https://doi.org/10.1016/j.rse.2020.112124).
- 720 Taucare, M., Viguier, B., Figueiroa, R., Daniele, L., 2024. The alarming state of Central Chile's groundwater resources: A  
 721 paradigmatic case of a lasting overexploitation. *Science of The Total Environment* 906, 167723. URL: <https://linkinghub.elsevier.com/retrieve/pii/S0048969723063507>, doi:[10.1016/j.scitotenv.2023.167723](https://doi.org/10.1016/j.scitotenv.2023.167723).
- 721 Tennekes, M., 2018. tmap: Thematic Maps in R. *Journal of Statistical Software* 84, 1–39. doi:[10.18637/jss.v084.i06](https://doi.org/10.18637/jss.v084.i06).
- 722 Urrutia-Jalabert, R., González, M.E., González-Reyes, ., Lara, A., Garreaud, R., 2018. Climate variability and forest fires in  
 723 central and south-central Chile. *Ecosphere* 9, e02171. URL: <https://esajournals.onlinelibrary.wiley.com/doi/10.1002/ecs2.2171>, doi:[10.1002/ecs2.2171](https://doi.org/10.1002/ecs2.2171).
- 724 Van Loon, A.F., Gleeson, T., Clark, J., Van Dijk, A.I., Stahl, K., Hannaford, J., Di Baldassarre, G., Teuling, A.J., Tallaksen,  
 725 L.M., Uijlenhoet, R., Hannah, D.M., Sheffield, J., Svoboda, M., Verbeiren, B., Wagener, T., Rangecroft, S., Wanders, N.,  
 726 Van Lanen, H.A., 2016. Drought in the Anthropocene. *Nature Geoscience* 9, 89–91. doi:[10.1038/ngeo2646](https://doi.org/10.1038/ngeo2646).
- 727 Venegas-González, A., Juñent, F.R., Gutiérrez, A.G., Filho, M.T., 2018. Recent radial growth decline in response to increased  
 728 drought conditions in the northernmost Nothofagus populations from South America. *Forest Ecology and Management* 409,  
 729 94–104. URL: <https://linkinghub.elsevier.com/retrieve/pii/S0378112717313993>, doi:[10.1016/j.foreco.2017.11.006](https://doi.org/10.1016/j.foreco.2017.11.006).
- 730 Venegas-González, A., Muñoz, A.A., Carpintero-Gibson, S., González-Reyes, A., Schneider, I., Gipolou-Zuñiga, T., Aguilera-Betti,  
 731 I., Roig, F.A., 2023. Sclerophyllous Forest Tree Growth Under the Influence of a Historic Megadrought in the  
 732 Mediterranean Ecoregion of Chile. *Ecosystems* 26, 344–361. URL: <https://link.springer.com/10.1007/s10021-022-00760-x>,  
 733 doi:[10.1007/s10021-022-00760-x](https://doi.org/10.1007/s10021-022-00760-x).
- 734 Vicente-Serrano, S.M., Azorin-Molina, C., Sanchez-Lorenzo, A., Revuelto, J., López-Moreno, J.I., González-Hidalgo, J.C.,  
 735 Moran-Tejeda, E., Espejo, F., 2014. Reference evapotranspiration variability and trends in Spain, 1961–2011. *Global  
 736 and Planetary Change* 121, 26–40. URL: <https://linkinghub.elsevier.com/retrieve/pii/S0921818114001180>, doi:[10.1016/j.gloplacha.2014.06.005](https://doi.org/10.1016/j.gloplacha.2014.06.005).
- 737 Vicente-Serrano, S.M., Beguería, S., López-Moreno, J.I., 2010. A multiscalar drought index sensitive to global warming: The  
 738 standardized precipitation evapotranspiration index. *Journal of Climate* 23, 1696–1718. URL: <http://dx.doi.org/10.1175/2009JCLI2909.1>, doi:[10.1175/2009JCLI2909.1](https://doi.org/10.1175/2009JCLI2909.1).
- 739 Vicente-Serrano, S.M., Peña-Angulo, D., Beguería, S., Domínguez-Castro, F., Tomás-Burguera, M., Noguera, I., Gimeno-Sotelo,  
 740 L., El Kenawy, A., 2022. Global drought trends and future projections. *Philosophical Transactions of the Royal Society A:  
 741 Mathematical, Physical and Engineering Sciences* 380, 20210285. URL: <https://royalsocietypublishing.org/doi/10.1098/rsta.2021.0285>, doi:[10.1098/rsta.2021.0285](https://doi.org/10.1098/rsta.2021.0285).
- 742 Vicente-Serrano, S.M., McVicar, T.R., Miralles, D.G., Yang, Y., Tomas-Burguera, M., 2020. Unraveling the influence of  
 743 atmospheric evaporative demand on drought and its response to climate change. *WIREs Climate Change* 11, e632. URL:  
 744 <https://wires.onlinelibrary.wiley.com/doi/10.1002/wcc.632>, doi:[10.1002/wcc.632](https://doi.org/10.1002/wcc.632).
- 745 Wickham, H., Averick, M., Bryan, J., Chang, W., McGowan, L.D., François, R., Grolemund, G., Hayes, A., Henry, L., Hester,  
 746 J., Kuhn, M., Pedersen, T.L., Miller, E., Bache, S.M., Müller, K., Ooms, J., Robinson, D., Seidel, D.P., Spinu, V., Takahashi,  
 747 K., Vaughan, D., Wilke, C., Woo, K., Yutani, H., 2019. Welcome to the tidyverse. *Journal of Open Source Software* 4, 1686.  
 748 doi:[10.21105/joss.01686](https://doi.org/10.21105/joss.01686).
- 749 Wilhite, D.A., Glantz, M.H., 1985. Understanding: The drought phenomenon: The role of definitions. *Water International* 10,  
 750 111–120. URL: <http://dx.doi.org/10.1080/02508068508686328>, doi:[10.1080/02508068508686328](https://doi.org/10.1080/02508068508686328).
- 751 Wilks, D.S., 2011. Empirical distributions and exploratory data analysis. *Statistical Methods in the Atmospheric Sciences* 100.
- 752 Winkler, K., Fuchs, R., Rounsevell, M., Herold, M., 2021. Global land use changes are four times greater than previously  
 753 estimated. *Nature Communications* 12, 2501. URL: <https://www.nature.com/articles/s41467-021-22702-2>, doi:[10.1038/s41467-021-22702-2](https://doi.org/10.1038/s41467-021-22702-2).
- 754 WMO, Svoboda, M., Hayes, M., Wood, D.A., 2012. Standardized Precipitation Index User Guide. WMO, Geneva. URL:

- 768        [http://library.wmo.int/opac/index.php?lvl=notice\\_display&id=13682](http://library.wmo.int/opac/index.php?lvl=notice_display&id=13682). series Title: WMO Publication Title: WMO-No.  
769        1090 © Issue: 1090.
- 770 Wright, M.N., Ziegler, A., 2017. ranger: A Fast Implementation of Random Forests for High Dimensional Data in C++ and  
771 R. Journal of Statistical Software 77, 1–17. doi:[10.18637/jss.v077.i01](https://doi.org/10.18637/jss.v077.i01).
- 772 Wu, C., Zhong, L., Yeh, P.J.F., Gong, Z., Lv, W., Chen, B., Zhou, J., Li, J., Wang, S., 2024. An evaluation framework  
773 for quantifying vegetation loss and recovery in response to meteorological drought based on SPEI and NDVI. Science of  
774 The Total Environment 906, 167632. URL: <https://linkinghub.elsevier.com/retrieve/pii/S0048969723062599>, doi:[10.1016/j.scitotenv.2023.167632](https://doi.org/10.1016/j.scitotenv.2023.167632).
- 775 Xiao, C., Zaehle, S., Yang, H., Wigneron, J.P., Schmullius, C., Bastos, A., 2023. Land cover and management effects on  
776 ecosystem resistance to drought stress. Earth System Dynamics 14, 1211–1237. URL: <https://esd.copernicus.org/articles/14/1211/2023/>, doi:[10.5194/esd-14-1211-2023](https://doi.org/10.5194/esd-14-1211-2023).
- 777 Yang, J., Huang, X., 2021. The 30 m annual land cover dataset and its dynamics in China from 1990 to 2019. Earth System  
778 Science Data 13, 3907–3925. URL: <https://essd.copernicus.org/articles/13/3907/2021/>, doi:[10.5194/essd-13-3907-2021](https://doi.org/10.5194/essd-13-3907-2021).
- 779 Zambrano, F., 2023. Four decades of satellite data for agricultural drought monitoring throughout the growing season in Central  
780 Chile, in: Vijay P. Singh Deepak Jhajharia, R.M., Kumar, R. (Eds.), Integrated Drought Management, Two Volume Set.  
781 CRC Press, p. 28.
- 782 Zambrano, F., Lillo-Saavedra, M., Verbist, K., Lagos, O., 2016. Sixteen years of agricultural drought assessment of the  
783 biobío region in chile using a 250 m resolution vegetation condition index (VCI). Remote Sensing 8, 1–20. URL: <http://www.mdpi.com/2072-4292/8/6/530>, doi:[10.3390/rs8060530](https://doi.org/10.3390/rs8060530). publisher: Multidisciplinary Digital Publishing Institute.
- 784 Zambrano, F., Vrieling, A., Nelson, A., Meroni, M., Tadesse, T., 2018. Prediction of drought-induced reduction of agricultural  
785 productivity in Chile from MODIS, rainfall estimates, and climate oscillation indices. Remote Sensing of Environment  
786 219, 15–30. URL: <https://www.sciencedirect.com/science/article/pii/S0034425718304541>, doi:[10.1016/j.rse.2018.10.006](https://doi.org/10.1016/j.rse.2018.10.006).  
787 publisher: Elsevier.
- 788 Zhang, W., Wei, F., Horion, S., Fensholt, R., Forkel, M., Brandt, M., 2022. Global quantification of the bidirectional de-  
789 pendency between soil moisture and vegetation productivity. Agricultural and Forest Meteorology 313, 108735. URL:  
790 <https://linkinghub.elsevier.com/retrieve/pii/S0168192321004214>, doi:[10.1016/j.agrformet.2021.108735](https://doi.org/10.1016/j.agrformet.2021.108735).
- 791 Zhao, Y., Feng, D., Yu, L., Wang, X., Chen, Y., Bai, Y., Hernández, H.J., Galleguillos, M., Estades, C., Biging, G.S., Radke,  
792 J.D., Gong, P., 2016. Detailed dynamic land cover mapping of Chile: Accuracy improvement by integrating multi-temporal  
793 data. Remote Sensing of Environment 183, 170–185. URL: <https://linkinghub.elsevier.com/retrieve/pii/S0034425716302188>,  
794 doi:[10.1016/j.rse.2016.05.016](https://doi.org/10.1016/j.rse.2016.05.016).
- 795 Zhou, K., Li, J., Zhang, T., Kang, A., 2021. The use of combined soil moisture data to characterize agricultural drought  
796 conditions and the relationship among different drought types in China. Agricultural Water Management 243, 106479. URL:  
797 <https://linkinghub.elsevier.com/retrieve/pii/S0378377420305965>, doi:[10.1016/j.agwat.2020.106479](https://doi.org/10.1016/j.agwat.2020.106479).